NASA

p_58

LABORATORY FOR HIGH ENERGY ASTROPHYSICS CONTRIBUTIONS TO THE 20TH INTERNATIONAL COSMIC RAY CONFERENCE

MOSCOW 1987

LABORATORY FOR HIGH ENERGY ASTROPHYSICS

NASA TM-
TM-92-T

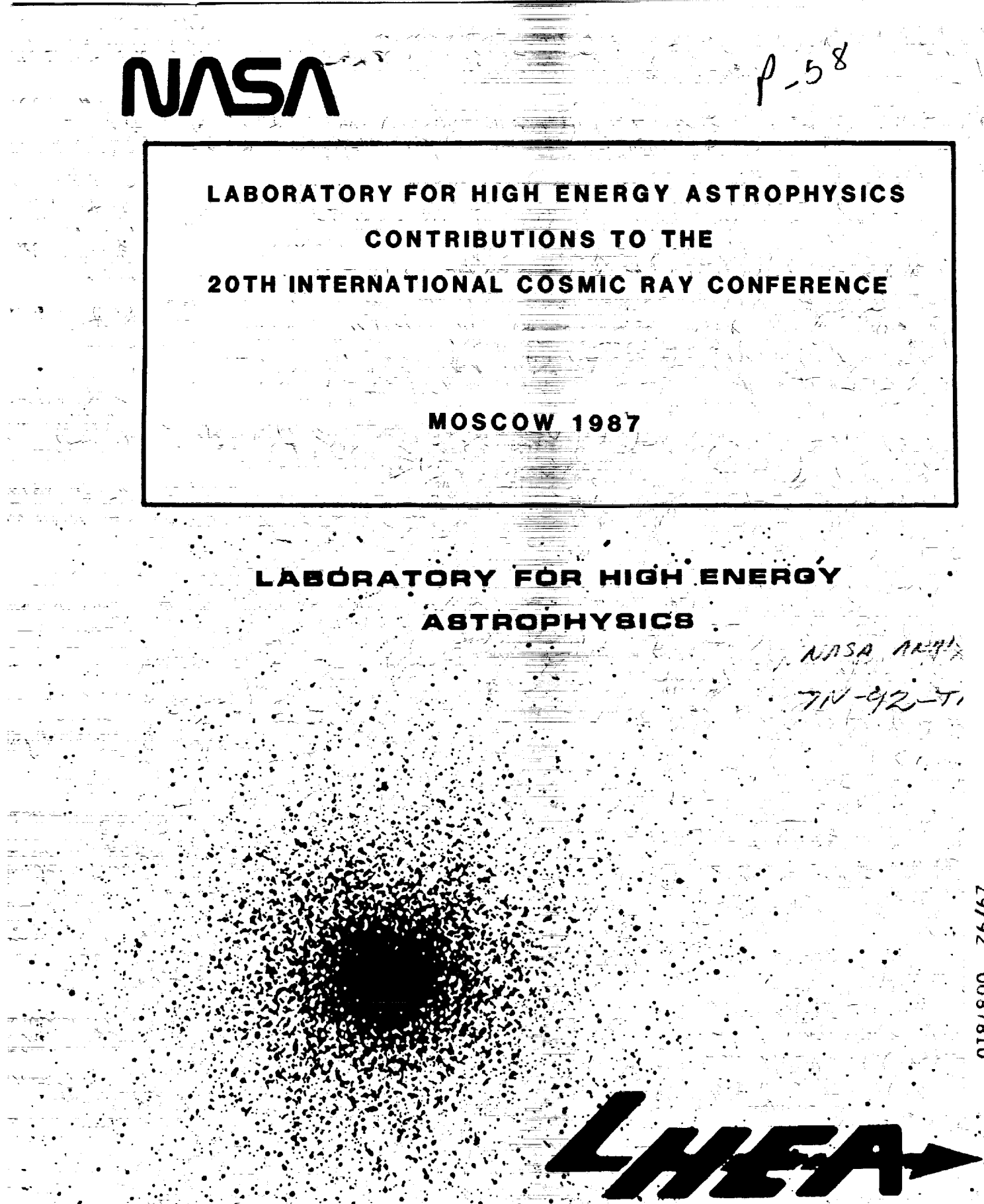

LHEA

National Aeronautics And Space Administration

Goddard Space Flight Center

Greenbelt, Maryland 20771

87-011

LABORATORY FOR HIGH ENERGY ASTROPHYSICS

CONTRIBUTIONS

TO THE

20TH INTERNATIONAL COSMIC RAY CONFERENCE

Moscow, U.S.S.R.

August 1987

To be published in the Proceedings

Table of Contents

Table of Contents

HARD X-Ray (Soft Gamma-Ray) Bursts and the 1979 March 5 Transient

T. L. Cline NASA/Goddard Space Flight Center, Greenbelt, MD, 20771, U.S.A.
C. Kouveliotou, Catholic University of America, Washington, DC, 20064, U.S.A.
J. Norris, Naval Research Center, Washington, DC, 20375, U.S.A.

Abstract

A series of transients from the galactic bulge direction has been observed to have energies intermediate between the X-ray burst and the gamma-ray burst domain. The events are distinct from the 'classical' gamma-ray bursts both in their repeating nature and in their characteristic energy; they are also very brief in duration. This brings to possibly four the historic total number of observed transient series of this type, including the 1979 March 5 event and its sequels, from the direction of N49 in the Large Magellanic Cloud (LMC), and Mazets' B1900+14 series and Babushkina's decade-old observation, both from the galactic disk. It is suggested that these repeaters, unlike the classical bursts with an isotropicaly distributed source pattern, have sources specifically in high-density galactic and the LMC regions. The evident similarity to the source distributions of X-ray binaries, infrared objects, and visible stars is discussed. The relative intensities and size spectra, the relationship to the anomalous 1979 March 5 event and other considerations are outlined.

1. Introduction. The recent discovery of a late-1983 cluster of soft transients adds a new aspect to the study of gamma-ray bursts. Several brief and spectrally soft transients in Prognoz-9 data records (1) were found to be within an extensive series of bursts having peak occurrence rate in November 1983: these events have a common source, also consistent with that of an earlier, January 1979 event in the galactic bulge (2). This new series of events is only the third case of a repeating group found with gamma-ray burst instrumentation; the other two consisted of at least 12 events observed from 1979 to 1982 (3,4) that were interpreted as sequel to the intense 1979 March 5 event and another group of three events in early 1979 (5). It is also possible that an unusually hard X-ray transient series seen with other instruments (6) may belong to this class. The newly discovered series, variously detected in Prognoz-9 (P-9), International Comet Explorer (ICE), and Solar Maximum Mission (SMM) data (7,8,9), are qualitatively similar to the others. With typically brief duration and lower characteristic energies, all appear to have a more elusive character than the 'classical' gamma ray bursts. It is thus possible that additional examples may be hidden in existing data.

The purpose of this note is to suggest a phenomenology that distinguishes soft repeaters from 'classical' gamma ray bursts. We find four basic differences: a, the spectral characters; b, the time histories; c, the source repetition natures; and d, the source direction patterns. Separating the two-event classes provides a simple resolution of the outstanding burst size spectrum puzzle and can favor the N49 source identification for the 1979 March 5 event, that which one of us has always supported (10,11,12).

2. Spectral and Temporal Properties. The spectrum of the January 7, 1979 event, apparently having a source in common with the 1983 repeater series (2), is qualitatively similar to those of the other repeater groups. All have

spectral character in the 30-keV region, well above that of X-ray bursts and equally well below that found for the hard gamma-ray bursts, the vast majority of which have been characterized in the 150-keV region since the beginning (13,14), with recently found extensions to many tens of MeV (15). This distinction alone is adequate to distinguish repeater events from the other kinds of transients. Time history, on the other hand, provides a statistically useful parameter: the hard bursts can have temporal durations over a very wide range, from the fractional seconds to at least 1 minute, as well as varying from simple to complex in temporal structure, whereas the soft events appear to be generally brief and simple. The SMM time history of the 01070 second UT, December 14, 1983 event is shown in Figure 1 as illustration (16).

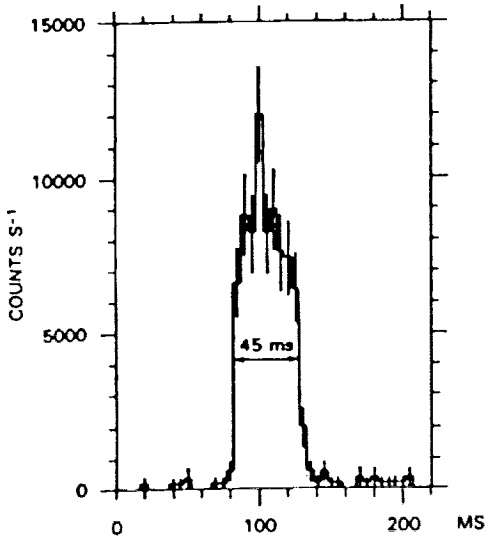

Fig. 1. The SMM observations of the 1983 December 14 event, recorded with 5 msec time resolution (16). This event was one of several tens of narrow events found in late 1983 from the galactic bulge direction (7,8,9).

3. Size Spectrum. One inconsistency in gamma-ray burst phenomenology consists of an observed cutoff in the burst size spectrum with an isotropic source distribution. Approaches to this problem range from the adoption of a galactic halo source region (17) to the redefiniton of 'size', using peak, rather than total, intensity (18). Also, it has been popular to credit misinterpretation of instrumental limitations as responsible, thereby dismissing the issue and permitting the views that source isotropy merely reflects a very nearby source volume. These approaches may be oversimplifications; at least, they have not taken into account the fact that small events are reliably detected as occurring in various series of repeaters. We believe that this second inconsistency--that of the detection of isolated groups of weak events with instruments that also give a cutoff in the size spectrum of isotropically distributed classical events--can be resolved by considering that gamma ray transients consist of two populations. Thus, given that the soft repeaters and the classical bursts qualitatively differ in their properties, instrument responses of entirely differing characters and biases could easily produce a severe distortion at the small-event end of the size spectrum of classical bursts while allowing for observations of low-intensity repeaters, with possible modifying effects yet to be uncovered.

4. Source Distribution. What we suggest here is the possibility of a fourth characteristic that may distinguish these two event classes. In addition to the hard versus soft spectral, complex versus simple temporal, and nonrepetitive versus repetitive emission properties, the source direction patterns are clearly separable. Gamma-ray bursts of the classical variety have been variously demonstrated to have an isotropic source pattern (e.g., 19). The source directions of the series of soft repeating events, on the other hand, can be interpreted to show a glimmer of an emerging pattern. Based on the 'counting rate statistics of three', of course, it is noteworthy

that the three repeaters have sources consistent with the galactic plane, with the galactic bulge near to the center, and with N49 in the nearby (by galactic dimensions) LMC. The plausibility of an emerging picture of repeating event origins in high-density (galactic or LMC) regions seems reasonable, making for a comparison of the familiar source patterns seen in starlight (visible from the southern hemisphere), in X-ray binaries and in the infrared. Figure 2 illustrates the gamma-ray transient repeater source locations (2,3,5) plotted with arrows on the galactic sky map of X-ray binaries (20).

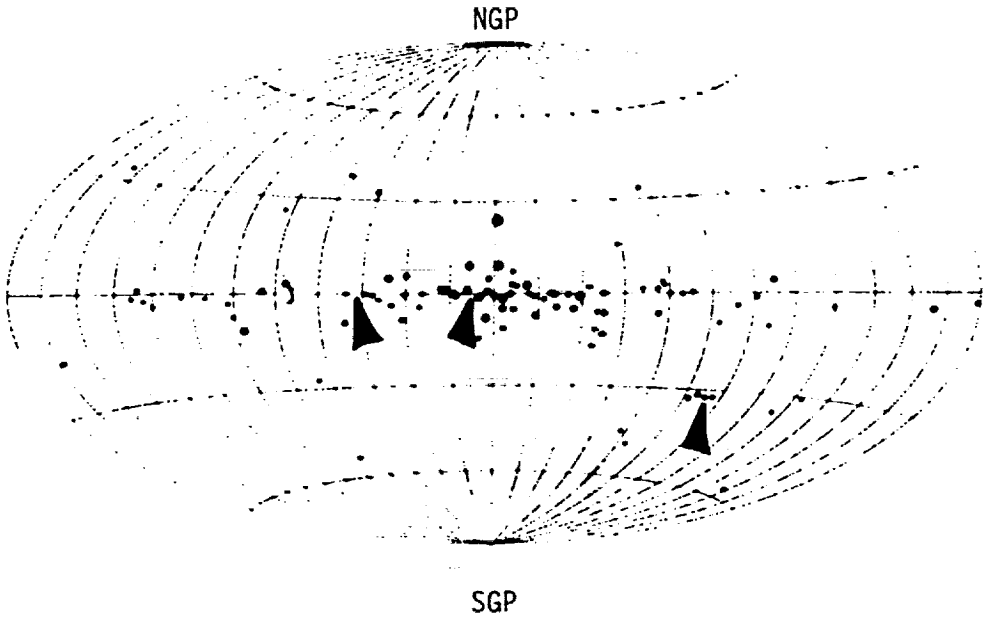

Fig. 2. The sources of the three known gamma-ray transient repeaters, plotted with arrows on a galactic map of X-ray binaries (20).

We can infer that the intensities of the galactic bulge events may be greater than those of the March 5 sequels since they are observed with less sensitive instrumentation. (The only instruments able to observe the March 5 sequels were not available for the recent, 1983 series, whereas some of the instruments observing this had at least been in use during the time of the March 5 sequels, but with null results. The directionality of some of these instruments is a complicating factor. The size spectrum of intensities from the bulge source (7,8) is still under study). This assumption, however, is consistent with the galactic center to LMC distance ratio; it thus can support the view that the March 5 sequel events have their source in the LMC.

5. March 5 Event Relationship. An outstanding puzzle regarding gamma-ray transients centers on the 1979 March 5 event. This burst differed in its properties from typical bursts in such detail that it could be described as forming a separate class (10). Its well-known periodicity (21,11) initially set it apart from other bursts and continues as the only clear example of

periodicity in gamma-ray bursts. (This distinction alone renders the assumption that this transient and 'classical' events have the same origin process as logically questionable.) The < 0.2 msec risetime (11) is an another anomalous characteristic that has remained particular to this event as the fastest of the hundreds logged before or since. The initial measurement of the source direction (22) gave a two arc-minute fit onto N49, with a refinement giving a much smaller field only seconds of arc from the center of that LMC supernova remnant (12). Despite this measurement, but because of the great relative intensity of this event, some models placed the source at a distance less than the galactic scale assumed for typical bursts, invoking an economy of assumptions to argue against considering this event to be in a distinct class.

We maintain that the positional agreement with N49 is surely too precise to be written off as 'accident' (given the number of snr's and pulsars and the way that this knowledge is figured in, the likelihood of chance coincidence is from 10^{-5} to 10^{-3} (11,23)). Clearly, the evidences for its anomalous nature (including its association with sequels, and its energy spectrum (21), like those of the sequels) argue against dismissing it as a bright, typical burst. The problem comes from the fact of the March 5 event itself: if the sequels alone had been observed--and the March 5 event circumstantially missed-- our suggestion of an LMC source for that series and disk sources for the others would be more straightforward. A recent model has put the LMC about a factor of 5 outside that calculated as possible for the March 5 event without gamma-ray beaming (24); perhaps such a requirement is not a strong constraint, given its rarity. We feel that the viewpoint outlined here may provide a clue towards further efforts for the understanding of gamma-ray transients.

References

1. K. Hurley, private communication.
2. J. Laros et al., 1986, Nature, 332, 152.
3. S. Golenetskii et al., 1983, A. F. Ioffe, Preprint No. 813.
4. E. Mazets et al., 1981, Nature, 290, 379.
5. E. Mazets and S. Golenetskii, 1979, A. F. Ioffe, Preprint No. 632.
6. O. Babushkina et al., 1975, Soviet Astron. Lett. 1, 1, 32.
7. K. Hurley et al., 1987, submitted to Ap. J. (Lett.).
8. J. Laros et al., 1987, submitted to Ap. J. (Lett.).
9. C. Kouveliotou et al., 1987, in preparation.
10. T. Cline, 1980, Comments Astrophys. 9, 13.
11. T. Cline et al., 1980, Astrophys. J. (Lett.) 237, L1.
12. T. Cline et al., 1982, Astrophys. J. (Lett.) 255, L45.
13. T. Cline et al., 1973, Astrophys., J. (Lett.) 185, L1
14. T. Cline and U. Desai, 1975, Astrophys. J. (Lett.) 196, L43.
15. S. Matz et al., 1985, Astrophys. J. (Lett.) 288, L37.
16. C. Kouveliotou et al., 1986, COSPAR Proceedings, Toulouse, France.
17. M. Jennings, 1985, Astrophys. J. 295, 51.
18. J. Higdon and R. Lingenfelter, 1986, Astrophys. J., in press.
19. J-L Atteia et al., 1987, Astrophys. J. Suppl., in press.
20. K. Wood et al., 1984, Astrophys. J. Suppl., 56, 507.
21. E. Mazets et al., 1979, Nature, 282, 279.
22. W. Evans et al., 1980, Astrophys. J. (Lett.) 237, L7.
23. J. Felten, 1981, 17th ICRC Proc., XG-2.2.
24. E. Liang, 1986, Astrophys. J. (Lett.), in press.

OBSERVATION OF GAMMA RAY LOW STATE OF CYGNUS X-1

J. Tueller, T. Cline, and B. Teegarden,
NASA/Goddard Space Flight Center, Greenbelt, MD, U.S.A.
W. Paciesas, University of Alabama at Huntsville, AL, U.S.A.
D. Boclet, P. Durouchoux, J. Hameury, CEN/Saclay, FRANCE
R. Haymes, Rice University, Houston, TX, U.S.A.

Abstract

Cygnus X-1 was observed on 25 September 1980 with a high-resolution cooled germanium spectrometer in the Low Energy Gamma-Ray Spectrometer (LEGS) balloon-borne experiment. The source was in a very low gamma-ray state; the differential flux at 45 keV was 1.3×10^{-3} ph/cm^2 sec keV. The results of a power law fit to our data are compared with three other observations (1,2,3) of a similar state. All of these spectra represent significantly lower gamma-ray fluxes than normally observed in the X-ray low or high state. Only HEAO-3 (1) has simultaneous X-ray data and, for that case, Cygnus X-1 was in the X-ray low state which normally corresponds to the highest gamma-ray emission. The similarity of the gamma-ray spectra suggest that all these measurements may correspond to the unusual state observed by HEAO-3 (1).

1. Introduction. The blackhole candidate, Cygnus X-1, is one of the brightest X-ray (1 keV to 10 keV) sources in the sky. The X-ray emission is normally in a low intensity state but several transitions to a high state, which can last weeks to months, have been observed. The high state is characterized by decreased gamma-ray (> 20 keV) emission as well as increased X-ray intensity. This behavior can be explained by an accretion disk model including the effects on the spectrum of comptonization by hot electrons to produce gamma-rays (8).

2. Observation. The LEGS experiment was configured with an array of three planar germanium detectors with an effective area of 53 cm^2 at low energies and resolution of 1.4 keV FWHM. An fine collimator made of iron restricted the field-of-view to 5° by 10° FWHM. A detailed description of the experiment has been published in Paciesas et al. (4). The source was observed for two 20-minute intervals at 3:16 UT and 5:57 UT. The average atmospheric depths including elevation correction for these two intervals were 5.9 g/cm^2 and 8.8 g/cm^2, respectively. Background data were accumulated before and after each source observation. A detailed description of data analysis procedures has been published in Tueller et al. (5).

3. Results. A narrow line search was performed from 20 keV to 400 keV, and no 3 sigma line candidates were detected. A search for the broad line feature reported by Watanabe (6) was performed. No broad lines in the region of 145 keV were observed, and our 3 sigma upper limit for a 14 keV FWHM line is 6×10^{-3} ph/cm^2 sec compared with the intensity reported in reference (6) of 1.3×10^{-2} ph/cm^2 sec. Since no narrow lines were observed, the data bins were chosen larger than the energy resolution to improve the statistical significance of individual points for display and fitting. Figure 1 shows the counts spectrum in the detector and data points extrapolated to the top of the atmosphere with error bars. This spectrum can be well fit by a power law with a reduced χ^2 1.3 for 11 d.o.f. Parameters for this fit are given in Table I. The single fluctuation at 47.5 keV and the slight excess above 100 keV are

not statistically significant. We can also achieve a good fit to our data with the comptonized model of Sunyaev and Titarchuk (7); however, we can only constrain the shape parameters with an upper limit on the optical depth (τ) and a lower limit on the electron temperature (kT_e). Figure 2 displays the confidence contours at two levels of significance for these parameters. Our data are consistent with the standard values (35 keV < kT_e < 50 keV and $1 < \tau < 5$) from Liang and Nolan (8).

4. Interpretation. Gamma-ray spectra with a soft spectral index ($\alpha > 2.2$) and low intensity have commonly been interpreted (8) as corresponding to the high X-ray state in the absence of X-ray measurements. Comparisons have been made with X-ray spectra monitored within a few days of the gamma-ray spectra. However, the source has been shown to include high states less than 4 days in total duration (9) and, therefore, only truly simultaneous measurements are conclusive. Only the measurement of HEAO-3 (1) has this simultaneous data, and it shows the source to be in the low X-ray state. There are no X-ray observations simultaneous with our observation. Measurements of the X-ray state by Ogawara et al. (9) on approximately 29 July and 12 October show the source in the low state but with erratic variations. The optical measurements of Kemp et al. (10) suggest that the source was in the X-ray low state at the time of our observation. On a balloon flight 10 days after ours, Frontera et al. (2) also observed the source in an extremely low gamma-ray state, which probably indicates a continuous decline between our two flights. Direct confirmation of the super low state first observed by HEAO-3 (1) requires simultaneous monitoring of the source at X-ray and gamma-ray energies. The available results are strongly suggestive that more sophisticated models may be required to explain the full range of variations observed in this source.

References

1. Ling et al., 1983, Ap. J., 275, p 307.
2. Frontera et al., 1985, Adv. Sp. Res., 5, p 125.
3. Matteson et al., 1976, Workshop on X-ray Binaries, NASA SP-389, p 407.
4. Paciesas et al., 1983, NIM, 215, p 261.
5. Tueller et al., 1983, Ap. J., 270, p 144.
6. Watanabe, 1985, Astro. and Sp. Sci., 111, p 157.
7. Sunyaev and Titarchuk, 1980, Astron. and Astrophys., 86, p 121.
8. Liang and Nolan, 1984, Sp. Sci. Rev., 38, p 353.
9. Ogawara et al., 1982, Nature, 245, p 675.
10. Kemp et al., 1981, Ap. J. Lett., 244, L73.

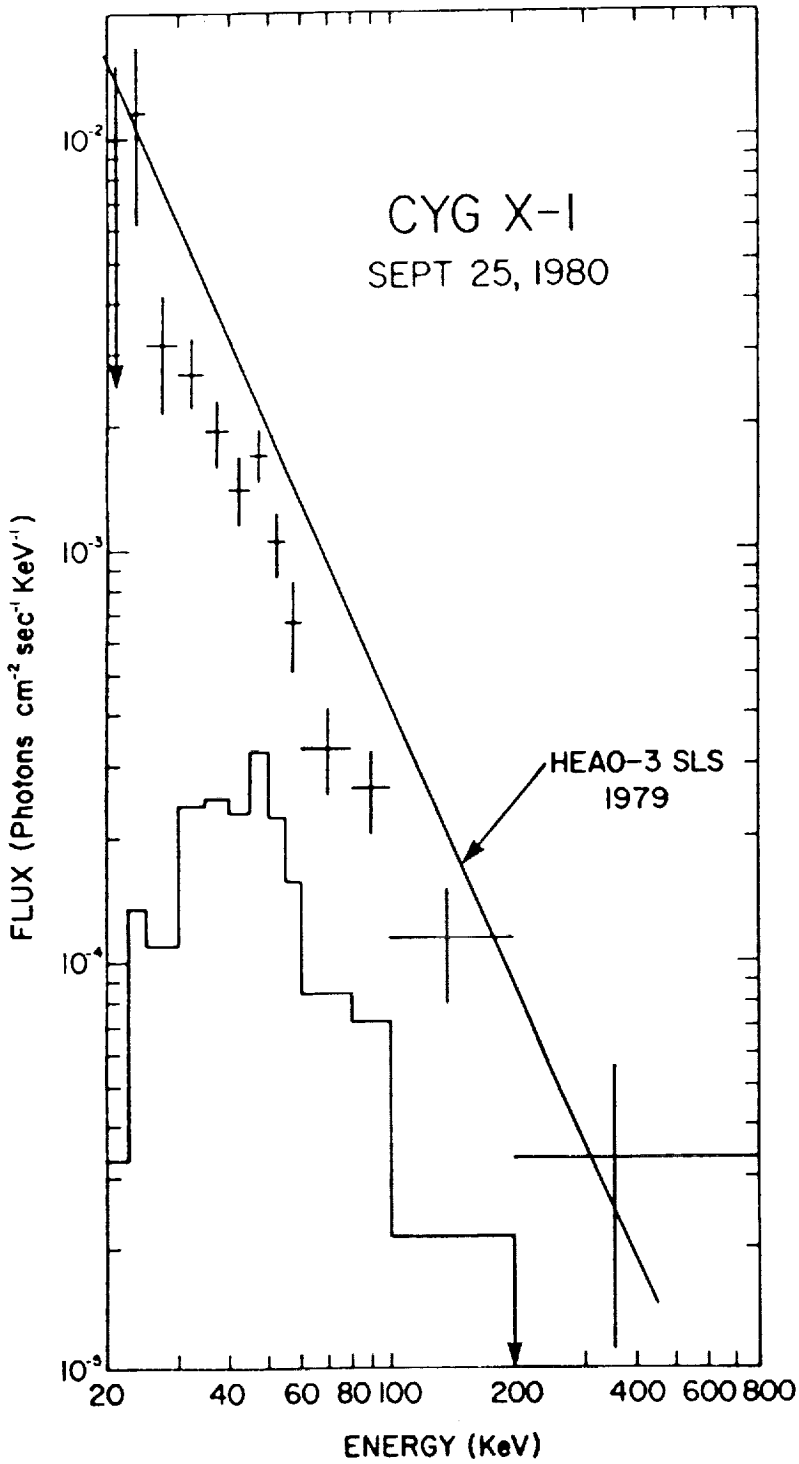

Fig. 1. Energy spectrum of Cygnus X-1. The data points are our results extrapolated to the top of the atmosphere. The histogram is the count rate at the detector showing the magnitude of the atmospheric correction. The solid line is a power law fit to the data of HEAO-3 (1) in September 1979 and shows that our results are a factor of two lower than the super low state.

TABLE I
$I(E) = I_0 (E/45)^{-\alpha}$

Date	I_0 (ph/cm^2 sec keV)	α	X-ray State	Reference
9/9/1970	0.6×10^{-3}	2.3	--	Matteson et al. (3)
9/1979	2.5×10^{-3}	2.24	Low	Ling et al. (1)
9/25/1980	$1.29 \times 10^{-3} \begin{smallmatrix} + 0.03 \\ - 0.05 \end{smallmatrix}$	2.3 ± 0.25	--	This experiment
10/4/1980	0.7×10^{-3}	2.7	--	Frontera et al. (2)

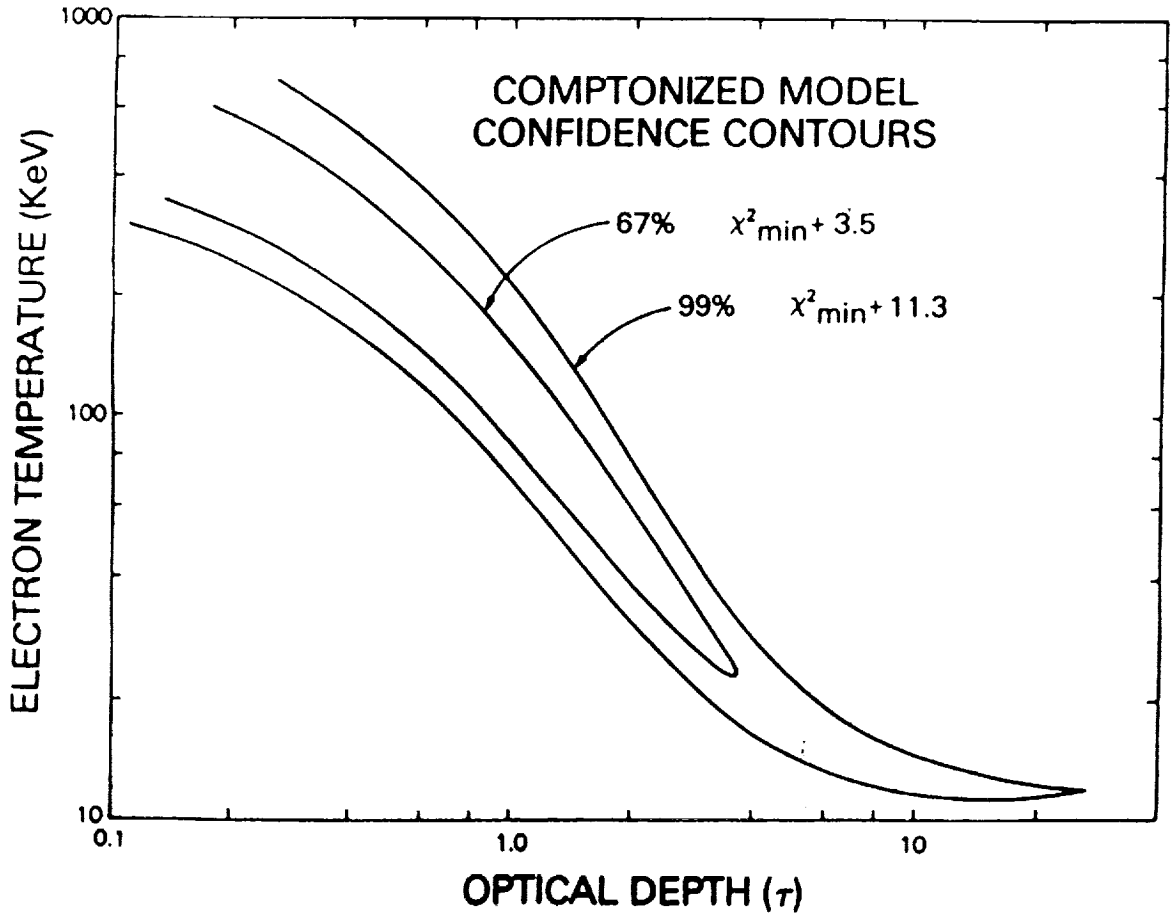

Fig. 2. Limits on the optical depth and electron temperature from fits with the comptonized spectrum model to our data.

ON THE POSSIBILITY OF OBSERVING COSMIC RAY SOURCES IN HIGH ENERGY GAMMA RAYS

J. F. Ormes, NASA/Goddard Space Flight Center, Greenbelt, MD 20771, U.S.A.

P. 4

Abstract

If cosmic rays are accelerated by strong shocks, then cosmic ray sources should be characterized by spectra, $dN/dE \alpha E^{-(2.0-2.2)}$, reflecting the strength of those shocks. This is expected from the "standard leaky box" model of cosmic ray propagation in which the source spectra are harder than the observed spectra because higher energy particles have shorter residence times in the galactic magnetic fields. Furthermore, data on cosmic ray nucleons suggest that these sources might be surrounded by material. If the latter is true, such sources should be observable in gamma rays at energies beyond 1 GeV where the angular resolution of γ-ray telescopes is optimized and the background is significantly reduced. For identified sources, the source location accuracy can be shown to improve with increasing energy in spite of the decreasing statistics, as long as the γ-ray spectrum is harder than $dN/dE \alpha E^{-\gamma}$. A Monte Carlo model is used to predict the photon spectra which would be expected from cosmic ray sources under varying assumptions about the strength of the shocks in the acceleration region.

1. Introduction. In this paper, characteristics of gamma-ray point sources in the energy range from 100 MeV to 1000 GeV are examined from the point of view of what is known from studies of heavy cosmic rays. These nuclei have lead to a picture of highly diffusive transport of nuclei through the interstellar medium, Cesarsky, 1980, and Cesarsky and Ormes, 1987 (1,2). The resulting pathlength distribution is exponential with the possibility that there exists a truncation at low pathlengths which physically could represent material around the cosmic ray sources. This is formalized in the nested leaky box model, Meneguzzi, 1973, and Cowsik and Wilson, 1973, (3,4) in which cosmic ray sources are surrounded by a shroud of matter with a mean pathlength of order 0.5 to 1.0 g/cm^2, Ormes and Protheroe, 1983, Garcia-Munoz et al., 1984, (5,6).

From these models and concomitant theoretical studies, a plausible mechanism for accelerating cosmic rays is the shock acceleration mechanism, Drury, 1983, (7). Strong shocks will produce spectra which are power laws in momentum, $dN/dE = k*p^{-(2.0 + \epsilon)}$, where ϵ depends on the strength of the shock. This implies that the spectra of cosmic rays at sources may well be much harder than those observed at Earth, and these spectra should be reflected in the spectra of photons at high energy. To date, all calculations of the neutral pion emissivity of the typical interstellar hydrogen atom has been based on the assumption that they are being bombarded by cosmic ray nucleons with spectra the same as those observed here at Earth.

2. Monte Carlo Simulations. Presented here are the results of a Monte Carlo simulation in which these sources are modeled, and the resultant gamma-ray emission is calculated. Thick and thin target cases have been considered as illustrated in Figure 1. Case I corresponds to a situation where a supernova sweeps up interstellar gas to form a thin shell of material surrounding a shock. Case II might correspond to a supernova producing a shock inside a preexisting cloud. Note that the column density in these cases

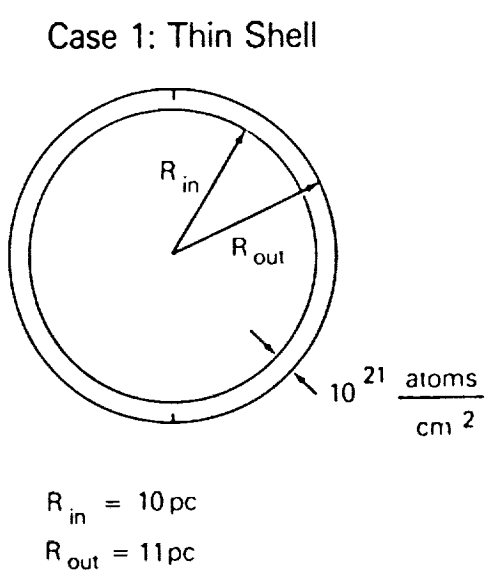

Fig. 1. The material in which the nucleous and electrons interact is localized in the shells indicated for the two cases. With a diffusion coefficient of the order 10^{26} cm^2 sec^{-1}, the effective thickness for the two cases are 1 and 10 g/cm^2.

is insufficient to account for the total grammage. It is assumed that the shells are filled with a highly tangled and diffusive magnetic field structure of the kind that is required to make the shock mechanism operable. Assuming a diffusion coefficient of the order 10^{26} cm^2 sec^{-1}, the grammages indicated can be reached.

Results from these models show that the photon spectrum is sensitive to the spectrum of incident nucleons in two respects. The harder the nucleon spectrum, the higher the emissivity per interstellar nucleon when integrated over the whole spectrum of incident nucleons. There is an enhancement factor based on the larger integral number, and the mean energy is higher leading to a higher pion multiplicity and, therefore, more secondary gamma rays. The harder cosmic ray spectrum is reflected in a harder photon spectrum above 300 MeV. These effects are shown in Figure 2 where the spectra of photons from various Monte Carlo runs are compared. The incident differential proton flux is taken to be the same at 100 MeV in all cases. The lower portion of Figure 2 shows the relative yield of photons from incident nucleon spectra of $p^{-2.7}$ and $p^{-2.0}$.

The upper portion of Figure 2 shows the relative photon spectra which result from nucleons accelerated in the interior of these two model cases. There are two effects here also. The thicker target yields more photons, but not quite in the ratio of the target thickness. Secondly, the thick target produces, below 100 MeV, secondary electrons through pi-mu-e decay which in turn produce Bremsstrahlung photons. Thus, as previously pointed out by Schlickheiser, 1982 (8), even if there are no primary electrons present, secondary electrons will mask the characteristic 70 MeV π° peak. Alternately, if sources could be found which are only evident above 100 MeV, these are candidates for thin shell sources.

We can estimate the fluxes which would be expected from such sources under the following assumptions:

1. Sources are at a distance such that they subtend an angle equal to the angular resolution of the telescope.

2. The differential nucleon intensities at 1 GeV are equal to those at Earth.

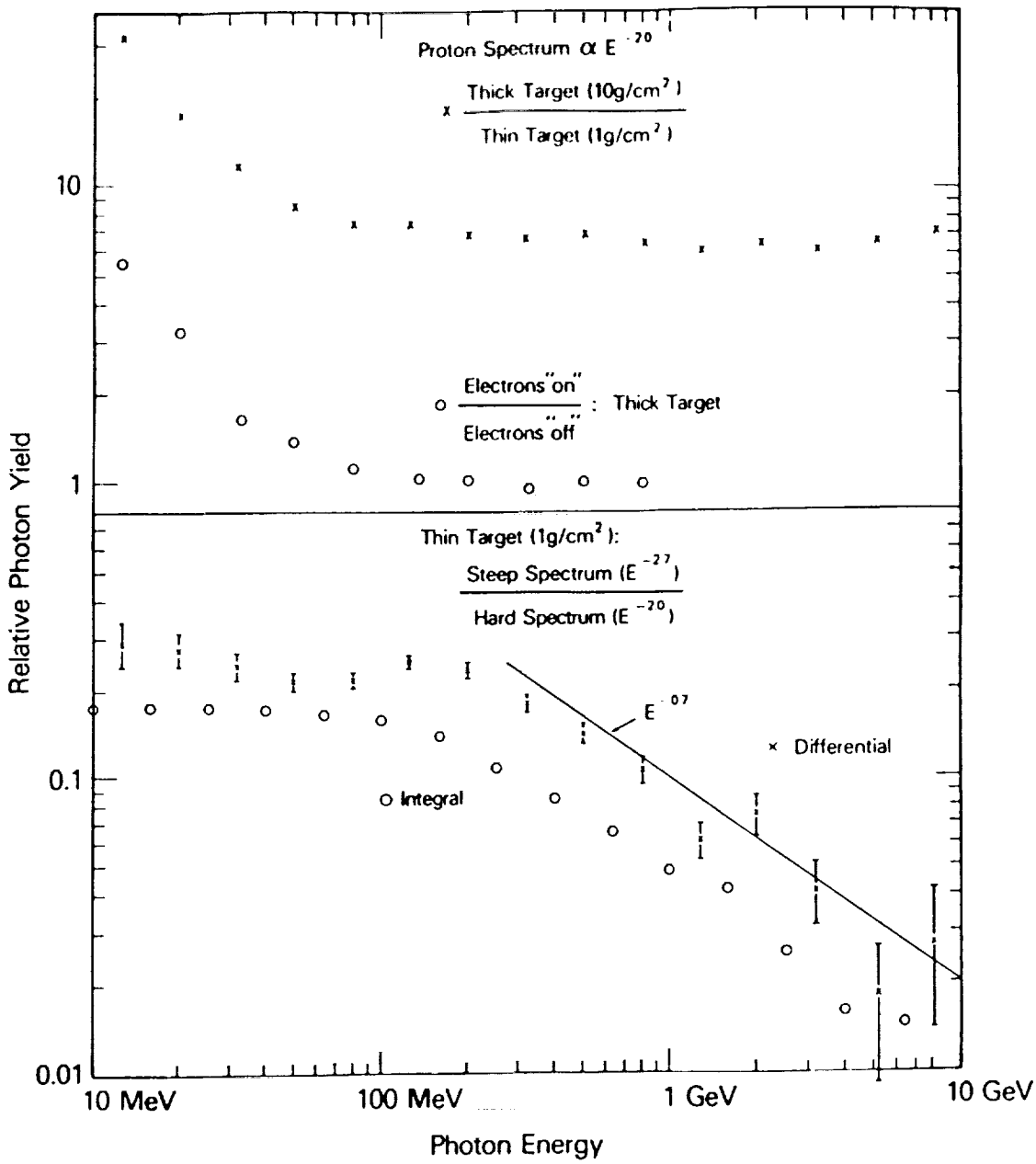

Fig. 2. Comparative photon yields are shown as a function of energy. The lower panel is for Case I, thin target, and shows the effect of different proton spectra. The upper panel compares the thick and thin target cases for a hard input particle spectrum.

For the thin target case, and a cosmic ray spectrum which has the same shape as observed at Earth, the intensity at Earth would be 3×10^{-7} cm^{-2} sec^{-1} which is below the COS-B sensitivity. However, for a cosmic ray source spectrum of E^{-2}, intensities of 1 or 2×10^{-6} cm^{-2} sec^{-1} are expected--intensities which would have been detected at the COS-B sensitivity limit. This conservative estimate for the flux is balanced by our optimism in placing these sources at a distance of 0.5 kpc. However, it is not unreasonable to assume that the intensity in the vicinity of a shock would be 10 to 100 times that in the average interstellar medium, in which case sources are potentially observable at the COS-B sensitivity limit out to 5 kpc.

3. Future Studies. Further work will be reported orally at the conference and in subsequent publications. This will involve studying the effects of including primary electrons (i.e., allowing the acceleration of electrons as well as nucleons by the shocks inside the clouds), the secondary production of positrons and antiprotons in such sources, and computing pathlength distributions for the nucleons leaving such sources. The sources in the COS-B data base will be studied to determine whether any of these data can be identified as possible candidate cosmic ray sources. However, there are severe constraints due to the statistical significance of the existing data, and a more complete analysis must await the improved data which will be available from EGRET.

References

1. Cesarsky, C. J., 1980, Ann. Rev. Astronomy and Astrophysics, 18, 289.
2. Cesarsky, C. J., and Ormes, J. F., 1987, Essays in Space Science, to be published.
3. Meneguzzi, M., 1973, Proc. 13th Int. Cosmic Ray Conf., 1, 378.
4. Cowsik, R., and Wilson, L. W., 1973, Proc. 13th Int. Cosmic Ray Conf. 1, 500.
5. Ormes, J. F., and Protheroe, R. J., 1983, Ap. J., 272., 756.
6. Garcia-Munoz, M., Guzik, T. G., Simpson, J. A., and Wefel, J. P., 1984, Ap. J. Lett., L13, 280.
7. Drury, L. O. C., 1983, Reports on Progress in Physics, 46, 973.
8. Schlickeiser, R., 1982, Astronomy and Astrophysics, L5, 106.

THE PULSAR CONTRIBUTION TO GALACTIC COSMIC RAY POSITRONS

Alice K. Harding and Reuven Ramaty
NASA Goddard Space Flight Center
Greenbelt, MD 20771, USA

Abstract

Measurements of high energy positrons in the cosmic rays appear to show an increase in the positron fraction above 10 GeV which is inconsistent with theoretical predictions of secondary positron production. We explore the possibility that observations of .1 - 1 GeV and Very High Energy (VHE) gamma-rays from the Crab and Vela pulsars could imply a significant primary positron contribution from galactic radio pulsars at energies above 10 GeV. Assuming that positrons are produced through magnetic pair creation in the cascades near the polar cap which may be the source of the observed gamma rays, we can estimate the flux and spectrum of the pulsar positron contribution. The pulsar positron component has a flatter spectrum than that expected from secondary cosmic ray production. The level of this contribution above 10 GeV is high enough to make pulsars viable sources of the high energy positron excess, and may also put interesting constraints on pulsar emission models.

1. Introduction. Positrons are expected in the cosmic rays as secondary products of interactions of cosmic ray nuclei with matter in the galactic disk. The positron flux has been measured[1,2,3] up to around 20 GeV. Above 10 GeV, these measurements indicate an excess over the predictions of secondary fluxes from cosmic ray interactions[4]. This could imply that a primary source of positrons becomes important above 10 GeV. While there may be multiple sources of both primary and secondary cosmic-ray positrons in the Galaxy, in this paper we determine the flux and spectrum of the pulsar component of primary positrons.

Radio pulsars are thought to be efficient accelerators of high energy particles through the induction of strong electric fields by a rotating magnetic dipole. Depending on the particular model, these fields may accelerate electrons or nuclei parallel to the curved magnetic field lines. The accelerated electrons radiate gamma rays through curvature radiation, which then produce electron-positron pairs in the magnetic field. These pairs radiate additional gamma rays through synchrotron radiation, which are capable of producing more pairs. The resulting cascade[5] may produce in excess of 10^4 pairs per primary particle which stream out of the pulsar magnetosphere into the surrounding nebula. The electron-positron pairs and gamma rays represent a significant fraction of the total spin-down energy loss of the pulsar. Positrons with energies up to 100 GeV have synchrotron radiation lifetimes greater than ~ 10^4 yr in a field of 10^{-4} G and thus could escape the surrounding supernova remnant without much energy loss.

Two of the youngest pulsars in the Galaxy, those in the Crab and Vela supernova remnants, are observed sources of gamma rays. At 100 MeV, they are among the strongest steady sources[6] and the highest energy emission is observed[7] sporadically by air Cherenkov arrays at 1000 GeV. Since these two are the youngest known pulsars, they are expected to be the strongest gamma-ray sources, but it is quite likely that many other pulsars are emitting gamma rays at levels below current detector sensitivities. The cascade models of pulsar gamma-ray emission predict that the pair spectrum should have about the same power law index and extend to nearly the same energies as the observed gamma rays. Therefore, pulsars should be sources of electrons and positrons in the Galaxy at energies up to 100 GeV. While their contribution to the primary electrons may be small, the contribution to the primary positron component could be significant.

We will evaluate the production rate and spectrum of primary positrons from the galactic population of pulsars, using observed gamma-ray fluxes and spectra of the Crab and Vela pulsars together with recent results on the galactic pulsar birthrate.

2. Pulsar Positron Production Rate. The observed (phase-averaged) flux of pulsed high energy gamma rays from the Crab pulsar up to ~ 1 GeV may be fit with the spectral form[8,9]:

$$\Phi_\gamma(E) = 2.4 \times 10^{-7}\ E^{-2.2}\ \text{ph cm}^{-2}\text{s}^{-1}\text{GeV}^{-1} \quad . \qquad (1)$$

where E is in GeV. The extrapolation of this spectrum to the VHE range (> 1000 GeV) falls above the existing data points[7], but could still be a reasonable approximation to the flux level at 10 - 100 GeV. Using Eqn (1) for the Crab pulsar flux, a distance of 2 kpc, an emission solid angle of 1 sr and a model for gamma-ray production in pulsars[10], the gamma-ray luminosity expected from any pulsar with rotation period P (in sec) and surface magnetic field strength B_{12} (in units of 10^{12} G) is:

$$L_\gamma(E) = 7.1 \times 10^{33}\ E^{-2.2} B_{12}\ P^{-1.7}\ \text{ph s}^{-1}\text{GeV}^{-1} \quad . \qquad (2)$$

This expression of course reproduces the value given in Eqn (1) for the parameters of the Crab (P = .033, B_{12} = 3.8) and is also consistent with the observed flux[8] of the Vela pulsar (P^2= .089, B_{12} = 3.4, d = 0.5 kpc).

We assume that all galactic pulsars emit gamma-rays like the Crab and Vela up to time t_{max}~ 10^4yr after their birth, and that positrons are produced with the gamma rays in pulsar cascades. Daugherty and Harding[5] have done numerical simulations of electromagnetic cascades which produce positrons and gamma rays in the polar cap regions of pulsars. In these simulations, the ratio of pairs to gamma rays is roughly .2 to .5 between 1 and 10 GeV for parameters needed to reproduce the observed Crab and Vela gamma-ray spectra. Since most of the positrons are produced with half the energy of the parent photon, the spectrum of positrons and gamma rays have the same spectral index. If f_+ is the ratio of positrons to gamma rays produced by a pulsar then the rate of positron emission is just f_+ times the gamma-ray luminosity given by Eqn (2).

We need to determine the total number of positrons which each pulsar will produce during its active lifetime. Using the spin-down formula which relates the period of a pulsar to its age t, $P \approx 2\dot{P}t$, and the electromagnetic dipole radiation formula which gives the magnetic field in terms of the period derivative $\dot{P}$ and period P, $B_{12} = 3.2 \times 10^7\ (P\dot{P})^{1/2}$, we obtain the rate of positron emission per pulsar as a function of time:

$$\frac{dN_+}{dt} = 2.3 \times 10^{46}\ f_+ B_{12}^{-0.7} t^{-.85}\ E^{-2.2}\ \text{s}^{-1}\text{GeV}^{-1}\text{pulsar}^{-1} \quad . \qquad (3)$$

As expected, younger pulsars have higher positron production rates. Integrating Eqn (3) gives the total number of positrons produced per pulsar over its gamma-ray emitting lifetime, t_{max}:

$$N_+(E) = 8.1 \times 10^{48}\ f_+ B_{12}^{-0.7} \left(\frac{t_{max}}{10^4\text{yr}}\right)^{.15}\ E^{-2.2}\ \text{GeV}^{-1}\text{pulsar}^{-1} \qquad (4)$$

which is consistent with an earlier estimate given by Arons[11]. In order to determine the total positron production rate in the Galaxy, we need the pulsar

birthrate. A recent determination of the pulsar galactic distribution[12] gives a rate of one pulsar every 30 to 120 yr in the Galaxy. In view of the large uncertainty in this number, we include a parameter, b_{30}, the pulsar birthrate normalized to a rate of 1/(30 yr). The total galactic positron production rate is then

$$Q_+(E) = 8.6 \times 10^{39}\, b_{30} f_+ B_{12}^{-0.7} \left(\frac{t_{max}}{10^4 yr}\right)^{.15} E^{-2.2}\ s^{-1} GeV^{-1} \quad . \qquad (5)$$

3. Comparison with Secondary Production by Cosmic Rays and Observations. The positron production rate by cosmic ray interactions per gram of interstellar gas in the energy range 1 to 100 GeV is[13,14],

$$q_{cr}(E) = 2.3 \times 10^{-3}\, E^{-2.7}\ e^+/(g\ s\ GeV). \qquad (6)$$

This spectrum is steeper than the prediction of Eqn (5) for the pulsar production rate. Combining Eqns (5) and (6), we obtain the total positron production rate per gram of interstellar matter,

$$q(E) = q_{cr}(E)\ [1 + k\ E^{0.5}], \qquad (7)$$

where

$$k = 0.37\ \frac{b_{30} f_+ (t_{max}/10^4 yr)^{0.15}}{(\ M\ /\ 5 \times 10^9 M_\odot)} \qquad (8)$$

and M is the total mass of interstellar gas. For k = 0.2 (b_{30} = 1, f_+ = .38, t_{max}= 10^5yr, M = 5 x $10^9 M_\odot$) the pulsar and cosmic ray contributions are equal at 25 GeV and at higher energies, the pulsar contribution dominates.

We have calculated the interstellar positron flux using Eqn (7) and the "leaky box" model with energy dependent escape path length 14 g cm^{-2} $E^{-0.55}$, which fits the results of ref. 15 from 3 to 30 GeV, and synchrotron and Compton energy loss rate

$$\frac{dE}{dx} = 1.5 \times 10^{-3}\left[0.6\left(\frac{B}{4 \times 10^{-6} G}\right)^2 + 0.4\left(\frac{w}{0.52\ eV\ cm^{-3}}\right)\right] E^2/n_H\ GeV\ cm^2 g^{-1} \quad . (9)$$

where E is in GeV. Here B is the perpendicular component of the interstellar magnetic field, w is the photon energy density, n_H is the hydrogen density and we assume an interstellar He abundance of 25% by mass. We take B = 4 x 10^{-6}G . The energy density of the 3K photon field is 0.25 eV/cm^3 and for the energy density in visible photons we take 0.45 eV/cm^3 with a factor of 0.6 to correct for the decrease in the Compton cross section at high energies. We take n_H = 0.25 cm^{-3}, consistent with an escape path length of 7 g/cm^2 at several hundred MeV/nucleon and an escape lifetime of 2 x 10^7yr (ref. 16).

The results are plotted in Figure 1 with k = 0.2 and compared with recent observations[2]. For reasonable parameters (see Eqn [8]) pulsars could account for the excess positron flux above that expected from cosmic ray interactions. The pulsar contribution has approximately the right spectral shape (a power law index slightly larger than 2.7) to fit the highest energy positron data. Given the uncertainties in the value of k, however, the pulsar positron flux could be lower than our estimate in Fig. 1.

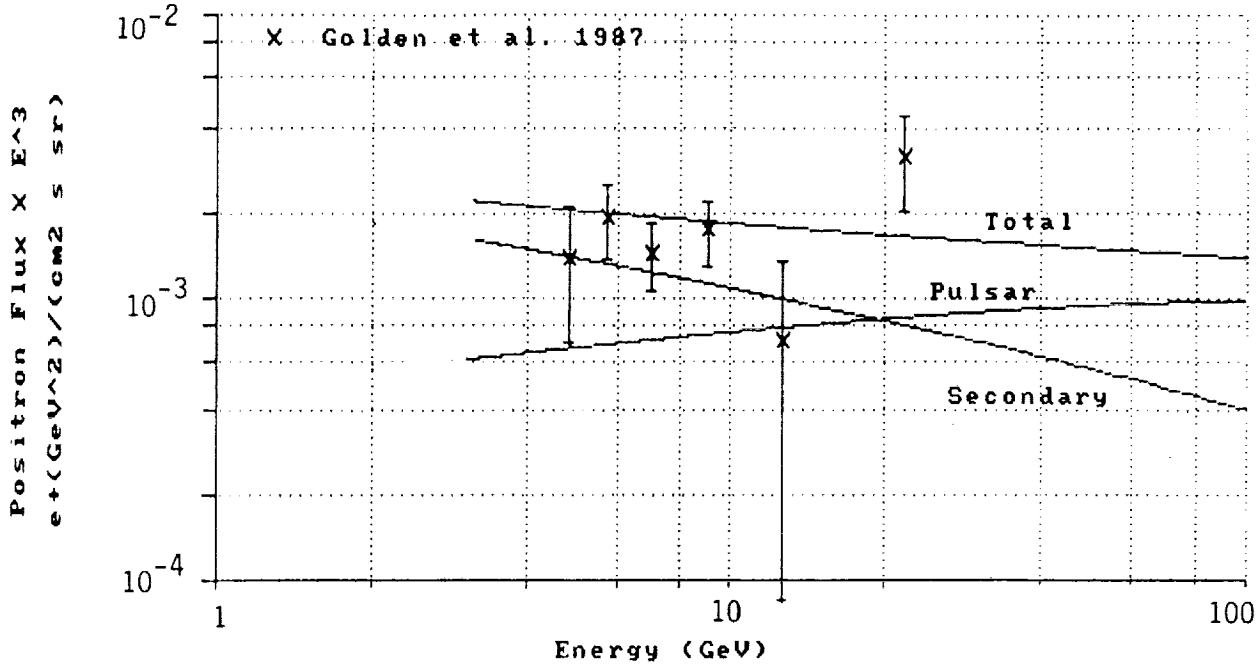

Figure 1. Predicted pulsar and secondary cosmic-ray positron flux between 3 and 100 GeV.

4. Conclusion. We have made an estimate of the spectral shape and flux of the high energy positron component due to pair production in radio pulsars. The major uncertainties in determining the pulsar contribution relative to other sources are the birthrate of pulsars in the Galaxy and the ratio of escaping positrons to observed gamma rays from pulsars. Additional uncertainties affecting all sources are introduced by parameters of the cosmic-ray propagation model. If pulsars become the dominant source of both electrons and positrons at high energies, then the ratio $e^+/(e^+ + e^-)$ should approach 0.5.

References

1. Golden, R. L. et al. 1985, 19th International Cosmic Ray Conf., 2, 374.
2. Golden, R. L. et al. 1987, preprint.
3. Muller, D. and Tang, J. 1985, 19th International Cosmic Ray Conf. Papers, 2, 378.
4. Protheroe, R. J. 1981, Ap. J., 251, 387.
5. Daugherty, J. K. and Harding, A. K. 1982, Ap. J., 252, 337.
6. Bennett, K, et al. 1977, Astr. Ap., 61, 279.
7. Tumer, O. T. et al. 1985, 19th International Cosmic Ray Conf. Papers, 1, 139.
8. Lichti, G. G. et al. 1980, Non-Solar Gamma Rays (COSPAR), ed. R. Cowsik and D. Wills, p. 49.
9. Knight, F. K. 1982, Ap. J., 260, 538.
10. Harding, A. K. 1981, Ap. J., 245, 267.
11. Arons, J. 1981, in IAU Symp. No. 94 "Origin of Cosmic Rays", ed. G. Setti, G. Spada and A.W. Wolfendale, (D. Reidel), p. 175
12. Lyne, A. G. , Manchester, R. N. and Taylor, J. H. 1985, Mon. Not. R. Astr. Soc., 213, 613.
13. Ramaty, R. and Westergaard, N. J. 1976, Astr. Sp. Sci., 45, 143.
14. Badhwar, G. D. and Stephens, S. A. 1977, 15th International Cosmic Ray Conference, 1, 398.
15. Ormes, J. F. and Protheroe, R. J. 1983, Ap. J., 272, 756.
16. Wiedenbeck, M. E. 1983, Composition and Origin of Cosmic Rays, ed. M.M. Shapiro (D. Reidel), p. 65.

ELECTRON HEATING IN A MONTE CARLO MODEL OF A HIGH MACH NUMBER, SUPERCRITICAL, COLLISIONLESS SHOCK

Donald C. Ellison[1,2] and Frank C. Jones[2]

[1]Astronomy Program
University of Maryland
College Park, Maryland 20742, USA

[2]Laboratory for High Energy Astrophysics, Code 665
NASA/Goddard Space Flight Center
Greenbelt, MD 20771, USA

1. Introduction. Energetic electrons are inferred to exist in many astrophysical environments. Examples include solar flares [where electron power laws in momentum to well above 10 MeV are observed (e.g. Evenson et al. 1984; Ellison and Ramaty 1985)], galactic cosmic rays [where electrons are observed to above 100 GeV (e.g., Tang 1984)], and the indirect evidence that electron acceleration occurs in supernova remnants (SNRs). In SNRs, the observed radio emission is best explained as synchrotron radiation from a continuously accelerated relativistic power law electron distribution. The fact that most SNRs are also X-ray emitters provides evidence that electron acceleration is associated with collisionless shocks.

Diffusive shock acceleration at quasi-parallel shocks (also called first-order Fermi shock acceleration) is often suggested as the mechanism for producing these energetic electron distributions. This results, in part, because diffusive acceleration, when applied to ions, has a strong theoretical basis (for reviews see Drury 1983; Forman and Webb 1985; Blandford and Eichler 1987), and has been extremely successful in explaining energetic ion populations in the heliosphere (e.g. Scholer 1985). It is not clear, however, if electrons can be readily accelerated at quasi-parallel shocks and, if so, with what efficiency. This is a particularly important question for those sites where inferred electron energy budgets are large since some considerations suggest that a much larger fraction of the shock energy (~ 100-1000 times) goes into the unseen protons.

Not only is electron acceleration problematical, but the mechanism for electron heating in quasi-parallel collisionless shocks is poorly understood.

In this paper, we present preliminary work in the investigation of electron injection and acceleration at parallel shocks. We describe a simple model of electron heating which is derived from the unified shock acceleration model of Ellison et al. (1981) and Ellison (1985) and which includes the effects of an electrostatic potential jump. Such a potential jump can lead to reflection of incident ions, an effect important for the understanding of oblique shocks.

The unified shock model provides a kinetic description of the injection and acceleration of ions and a fluid description of electron heating at high Mach number, supercritical, parallel shocks. The ion dissipation results when the directed ion kinetic energy is randomized by elastic and isotropic scattering by infinitely massive scattering centers which represent Alfvenic fluctuations in the converging flows; the thermal or random pressure of the ions increases at the expense of the ram pressure when a discontinuity in the flow is crossed. If only protons are present, the elastic scattering insures that the increase in random pressure balances the decrease in ram pressure and the Rankine-Hugoniot (R-H) conservation conditions are satisfied. When thermal electrons are included, the Mach number decreases and, in order to satisfy the R-H conditions, the electron fluid must be heated.

2. Model. To determine this heating, we calculate the pressure increase protons receive after crossing a discontinuity in the flow velocity, u, that is not necessarily a shock transition, i.e., momentum flux need not be conserved. The particles cross from region I to region II and energy is conserved when viewed from frame II. Therefore, the energy flux across the transition from region I to region II, $J_{I\to II}$, is given by

$$J_{I\to II} = \Delta u(\tfrac{1}{2}\rho_I \Delta u^2 + \frac{\gamma}{\gamma-1} P_I) \tag{1}$$

where ρ_I and P_I are the density and pressure of the plasma in region I, γ is the ratio of specific heats, and $\Delta u = u_I - u_{II}$ is the change in flow velocity.

The energy density in region II after the transition has passed, ϵ_{II}, is equal to the energy density before the transition has passed, ϵ_I, plus the change in energy density produced by the transition, $\Delta\epsilon_{I\to II}$, i.e., $\epsilon_{II} = \epsilon_I + \Delta\epsilon_{I\to II}$ where $\Delta\epsilon_{I\to II} = J_{I\to II}/u_{II}$. Therefore,

$$\epsilon_{II} = \frac{1}{2}\rho_I \Delta u^2 + \frac{P_I}{\gamma-1} + \frac{\Delta u}{u_{II}}(\tfrac{1}{2}\rho_I \Delta u^2 + \frac{\gamma}{\gamma-1} P_I) \tag{2}$$

and the pressure in region II is given by,

$$P_{II} = (\gamma-1)\epsilon_{II} = \frac{\gamma-1}{2}\rho_I \Delta u^2 \frac{u_I}{u_{II}} + P_I(\gamma\frac{u_I}{u_{II}} - \gamma + 1). \tag{3}$$

For a shock transition in an electron-proton plasma, the R-H conditions relate the upstream and downstream plasma parameters. In particular they provide $P_2/P_1 = (2\gamma M_1^2 - \gamma + 1)/(\gamma+1)$, where $P_1 = P_{e1} + P_{p1}$ ($P_2 = P_{e2} + P_{p2}$) is the sum of the upstream (downstream) electron and proton pressures, and $M_1 = \sqrt{[\rho_1 u_1^2/(\gamma P_1)]}$ is the sonic Mach number. The subscripts 1 (2) indicate upstream (downstream) values when the transition is a shock. The R-H conditions give no information on the distribution of pressure between electrons and protons. Such information, since it depends on microprocesses, can not be predicted by fluid theories and must be determined with a kinetic description of the shock. For a shock, Eq. (3) gives

$$P_{e2} + P_{p2} = \frac{\gamma-1}{2}\rho_1 \Delta u^2 r + (P_{e1} + P_{p1})(\gamma r - \gamma + 1) \tag{4}$$

where $r = u_1/u_2$ is the shock compression ratio. In our simulation, protons are treated explicitly and are scattered elastically in the local plasma frame. Therefore, Eq. (3) holds for protons individually, i.e.,

$$P_{p2} = \frac{\gamma-1}{2}\rho_1 \Delta u^2 r + P_{p1}(\gamma r - \gamma + 1) \ . \tag{5}$$

Substracting Eq. (5) from (4) we have

$$P_{e2}/P_{e1} = \gamma r - \gamma + 1 \ . \tag{6}$$

Eq. (6) describes the electron dissipation required if protons are dissipated by elastic scattering in the downstream plasma frame. The change in entropy for electrons is $\Delta S \propto \log[(\gamma r - \gamma + 1)/r^{\gamma}]$ and is always less than zero, indicating that electrons are heated less than if they were adiabatically compressed. This

implies that additional electron dissipation is required to satisfy basic thermodynamic considerations. Below we consider the effects of an electrostatic potential jump.

Equation (6) applies when no potential jump exists. To calculate the effect of an electrostatic potential jump at the shock, we assume a potential, Φ, exists such that protons are slowed upon crossing the shock, i.e., (for high Mach numbers and for Φ small enough such that an insignificant fraction of protons is reflected)

$$u_3^2 \simeq u_1^2 - \frac{2e\Phi}{m_p} \qquad (7)$$

where u_3 is the flow velocity of the protons after they cross the potential jump but before they make their first "collision" downstream. The proton pressure in the downstream region, P_{p2}, is obtained from Eq. (3) by making the replacements $P_I \rightarrow P_{p3}$, $\rho_I \rightarrow \rho_3$, and $u_I \rightarrow u_3$. In the high Mach number limit, the mean energy per proton is conserved, therefore $P_{p3}/\rho_3 \simeq P_{p1}/\rho_1$ and, since $\rho_3/\rho_1 = u_1/u_3$, we can replace P_{p3} by $(u_1/u_3)P_{p1}$. With this substitution, the downstream proton pressure is determined by upstream quantities and the increase in downstream pressure necessary to compensate for the reduced proton pressure, ΔP_Φ, is given by,

$$\Delta P_\Phi = \frac{\gamma-1}{2}\rho_1 r\,[u_1^2 - u_3^2 - 2u_2(u_1 - u_3)] + P_{p1}[\frac{u_1}{u_3}(\gamma-1) - \gamma + 1] \; . \qquad (8)$$

Therefore, within the context of our model, there are two distinct sources of electron heating. The first (given by Eq. 6) is the heating required to compensate for the reduced proton heating when the addition of an upstream electron pressure lowers the shock compression ratio. The other source results from an electrostatic potential jump when we assume that the energy lost by protons upon crossing the potential goes into electron pressure. This increase in downstream electron pressure is given by Eq. (8). In both cases, we calculate the increase in electron pressure necessary to satisfy the R-H conditions when the proton pressure is decreased.

3. Summary. In the Figure we show the downstream to upstream pressure ratios for electrons and protons versus M_1 and for different values of $e\Phi/(m_p u_1^2) \equiv \phi$. For plots (a), $\phi = 0$, for plots (b), $\phi = 0.05$, and for plots (c), $\phi = 0.1$. This calculation assumes that $T_{p1} = T_{e1}$, $\gamma = 5/3$, and it is noted that the assumptions leading to Eq. (8) are only strictly valid at high Mach numbers. It is clear from this figure that electron heating can depend strongly on an electrostatic potential jump. The dotted line is the line of constant electron entropy. For curves that lie below this line, electrons lose entropy in the shock. Realistic models must lie above the line, indicating the necessity for a potential jump.

References

Blandford, R.D., and Eichler, D., 1987, Physics Reports, in press.
Drury, L. O'C, 1983, Rep. Prog. Phys., 46, 973.
Ellison, D.C., 1985, J. Geophys., Res., 90, 29.
Ellison, D.C., Jones, F.C., and Eichler, D., 1981, J. Geophys., 50, 110.
Ellison, D.C., and Ramaty, R., 1985, Ap. J., 298, 400.
Evenson et al., 1984, Ap. J., 283, 439.
Forman, M.A., and Webb, G.M., 1985, in Collisionless Shocks in the Heliosphere, eds. R.G. Stone & B.T. Tsurutani, Geophysical Monograph Vol. 34, p. 91.
Scholer, M., 1985, in Collisionless Shocks in the Heliosphere, eds. R.G. Stone & B.T. Tsurutani, Geophysical Monograph Vol. 35, p. 287
Tang, K.K., 1984, Ap. J., 278, 881.

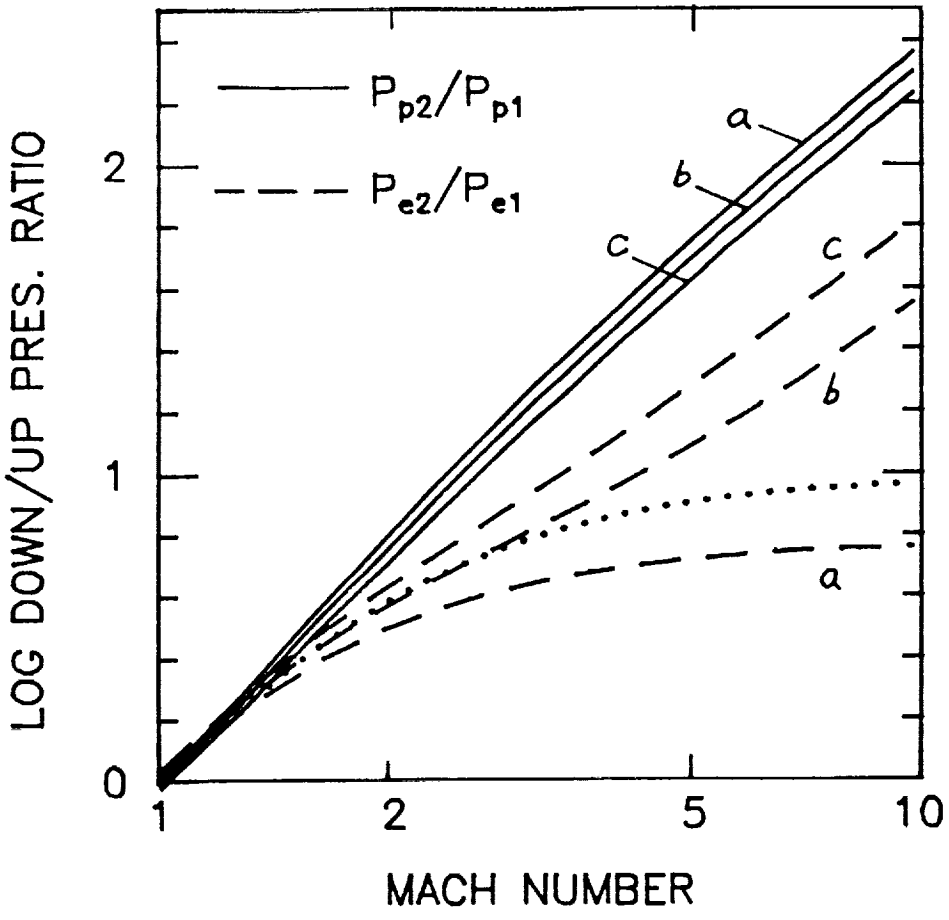

Fig. 1. Ratio of downstream to upstream pressure vs. Mach number. Solid lines show the proton ratio and the dashed lines show the electron ratio. The two curves labelled (a) are for no potential jump, those labelled (b) are for $e\varphi/(m_p u_1^2)$ = 0.05, and those labelled (c) are for $e\varphi/(m_p u_1^2)$ = 0.1. The dotted line assumes the electrons are adiabatically compressed, i.e., $P_{e2}/P_{e1} = r^{\gamma}$.

OG-9.2-5 56-19
N92-70640
p. 4

A PARTICLE ASTROPHYSICS MAGNET SPECTROMETER FACILITY FOR SPACE STATION

J. F. Ormes, NASA/Goddard Space Flight Center, Greenbelt, MD., U.S.A.
M. H. Israel, Washington University, St. Louis, MO., U.S.A.
R. Mewaldt, Caltech, Pasadena, CA., U.S.A.
M. Wiedenbeck, University of Chicago, Chicago, IL., U.S.A.

Abstract

Planning for and design tradeoff studies related to the particle astrophysics magnet spectrometer known as Astromag (1) will be presented. This facility is being planned for the Space Station and will address questions regarding the origin and acceleration of cosmic rays, explore the synthesis of elements by making detailed measurements of cosmic ray isotopic composition, and search for evidence of antimatter and other cosmologically significant particles. This work has been supported by an international study team which includes particle physicists and cosmic ray physicists (see List of Names at the end of paper).

1. Introduction. Observations over the past several years have given unexpected results on the elemental and isotopic composition of cosmic-ray nuclei and on the cosmic-ray abundances of antiprotons and positrons. Theoretical developments suggest the acceleration of these particles by strong shocks in the interstellar medium. These results have raised new questions about the origins of energetic particles in astrophysical settings, sometimes deeply related to fundamental questions of astrophysics, cosmology and elementary particle physics. For example: What is the source of the large abundances of antiprotons observed in the cosmic radiation? Is there evidence for known or unknown particles which could account for missing mass in the universe? What is the nucleosynthetic history of this sample of non-solar system material? What is the origin of relativistic particle plasma in the galaxy, and what are its effects on the dynamics and evolution of the galaxy? Answering these questions requires long space exposures of large instruments; the development of a permanently manned Space Station offers the opportunity to perform the needed experiments.

Over the past year the Particle Astrophysics Magnet Facility (Astromag) Definition Team has examined how a large magnetic spectrometer outside the Earth's atmosphere for an extended period of time could address these questions. A facility, composed of a core magnet, dewar, and associated support equipment would be used to conduct a series of experiments using a variety of instrumentation. A number of magnet and instrument configurations have been considered, and it appears to be quite feasible to construct and operate such a spectrometer facility on the Space Station. The scientific objectives that could be addressed by this facility are summarized and a "strawman" configuration of magnet and instruments capable of achieving some of those objectives is described. Other objectives could be achieved by changing and reconfiguring the instrument complement used in conjunction with the magnet.

2. Measurements. The scientific objectives of Astromag will be met with particle detection instruments designed to make the following observations:

- o Search, with unprecedented sensitivity, for anti-nuclei of helium and heavier elements--The identification of any such anti-nuclei would imply that the Universe contains domains of antimatter and would have profound cosmological implications.

- o Measure the spectra of anti-protons and positrons--These anti-particles have already been seen in the cosmic rays, and they are expected as secondary products of primary cosmic-ray interactions with the interstellar gas; however, antiproton fluxes are higher than expected from normal models of galactic cosmic-ray propagation. Further investigation of these spectra will surely improve our understanding of the origin of cosmic rays and may lead to the discovery of processes unpredictable from present knowledge of elementary particle physics and cosmology.

- o Measure the isotopic composition of cosmic-ray nuclei at energies of several GeV/amu (higher than reached by other means) and with previously unattained sensitivity--The few reliably measured elements show that the isotopic composition at the cosmic-ray source is different from that of ambient material found in our solar system. Distinguishing among models of cosmic-ray sources which might explain these differences requires isotopic composition measurements of many other elements at different energies and with much greater sensitivity than presently achieved. In addition, measurement of radioactive isotopes over a range of Lorentz factors will answer questions about the storage of cosmic rays in the galaxy.

- o Measure the energy spectrum of cosmic ray nuclei to very high energies with unprecedented precision--Spectral differences between primary and secondary nuclei are indicative of galactic confinement processes and can lead to the determination of source abundances of rare elements. Fine structure in the energy spectra, if observed, would revolutionize ideas about the origin of cosmic rays.

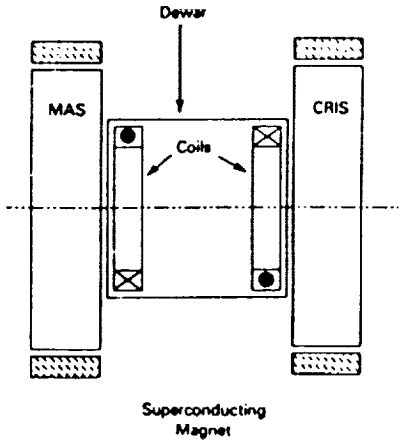

Fig. 1. Schematic of Astromag. The Matter Antimatter Spectrometer (MAS) and the Cosmic Ray Isotope Spectrometer (CRIS) are indicated in the two experimental regions.

3. The Magnet Spectrometer and Instruments. The heart of the Astromag system is the superconducting magnet Green et al., 1986, (3). The sign and magnitude of the deflection in the high magnetic field are measured by high precision particle tracking detectors. A variety of coil configurations have been considered. The final choice will be based on studies of performance yet to be performed.

To undertake the variety of observations listed above, at least two different detector configurations will be required; one for protons, electrons, and the other low-charge particles and another for higher charged nuclei. The instrumentation for Astromag will be mounted in two separate sections as shown in the "strawman" configuration in Figure 1. This configuration provides two prime locations for instrumentation, just outside each coil. The magnet consists of

two circular coils, each about 2 m in diameter and separated by about 2 m, inside a single cylindrical dewar. Currents in the two coils have opposing senses, so the overall system has no net dipole moment and thus does not exert any significant torques on the Space Station.

At the edge of the Astromag detectors, about 2 meters from the coils, the magnetic induction would be about 2000 Gauss (0.2 Tesla). The field falls to 25 Gauss between 6 and 8 m from the coils and falls below 1 Gauss between 16 and 18 m. The liquid helium to keep the coils in the superconducting state requires periodic helium resupply every 12 to 24 months. Mounting this facility on the Space Station, where a manned presence and frequent visits by the Shuttle are planned, will facilitate this resupply.

Safety considerations for superconducting magnets are now well understood, as a result of their widespread use in terrestrial laboratories. The system will be designed to withstand without damage the sudden collapse of the magnetic field and the dissipation of that energy. This contingency would occur if the liquid helium were suddenly lost or if for any other reason the conductor made the transition from the superconducting state to the normal state.

The basic magnet facility measures the magnetic rigidity of charged particles. The precision of this measurement is characterized by the maximum detectable rigidity (R_{max}) which depends directly on the field integral and inversely on the positional error measuring devices. Given position detectors with 50 μm resolutions, the geometric factor shown in Figure 2 results.

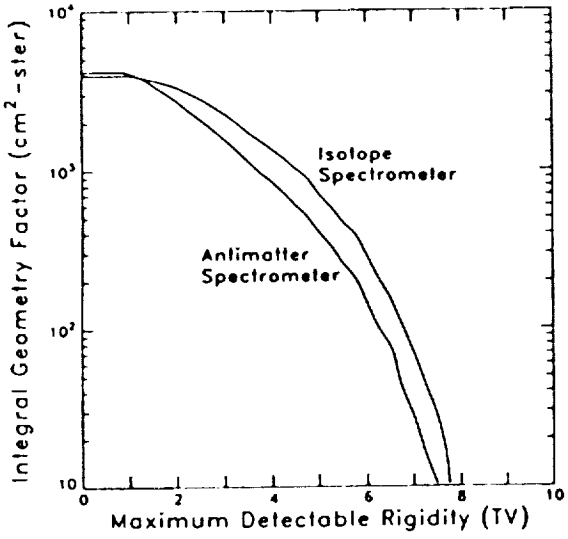

Fig. 2. The geometric factor as a function of R_{max}.

Candidates for the high and low charge trajectory measuring detectors are, respectively, Multiwire Proportional Counters (MWPC) (3) and Scintillating Optical Fiber Trajectory (SOFT) (4) detectors. Each can achieve resolution in the range of 50 μm, while introducing such small amounts of material into the particle path that the resolution is not degraded by multiple Coulomb scattering of the particle. MWPC's have been successfully used with magnetic spectrometers for singly charged particles, and SOFT detectors have achieved this resolution in the laboratory with iron nuclei.

The Matter-Antimatter Spectrometer consists of instruments optimized for protons, antiprotons, electrons, and positrons over an energy range from a few GeV to about a TeV. It will make both high precision measurements of energy spectra of low-Z elements from a few GeV/amu to a few hundred GeV/amu and high-resolution measurement of gamma rays with energy between about 1 and 100 GeV. It will also conduct high sensitivity searches for antinuclei with atomic number 2 to 10 at energies above a few GeV/amu.

At the other end is a Cosmic Ray Isotope Spectrometer . CRIS is optimized for measurement of the isotopic composition of elements with atomic number 6 to 28 at energies of several GeV/amu and for searches for antinuclei pt energies above a few GeV/amu. In addition to the basic magnetic spectrometer, CRIS uses Cherenkov counters of various indices of refraction to measure the charge and velocity of the incident particles.

References

1. Ormes, J. F., Israel, M. Wiedenbeck, M. and Mewaldt, R., "The Particle Astrophysics Magnet Facility, Interim Report, 1986, NASA, Code 661, Greenbelt, MD, 10771, U.S.A.
2. Astromag: A Superconducting Particle Astrophysics Magnet Facility for the Space Station, M. A. Green, G. F. Smoot, R. L. Golden, M. H. Israel, R. Kephart, R. Niemann, R. A. Mewaldt, J. F. Ormes, P. Spillantini, and M. E. Wiedenbeck, Proc. of IEEE Conference on Applied Superconductivity, Baltimore, 1986.
3. Golden et al., 1978, Nucl. Instrum. and Methods, 148, 179.
4. Binns et al., 1986, Nucl. Instrum. and Methods, A251, 402 and 1987, Nucl. Instrum. and Methods, in press.

ASTROMAG FACILITY DEFINITION TEAM

Astromag Definition Team Members:

Theodore Bowen, University of Arizona
Robert L. Golden, New Mexico State University
William Hibbard, NASA/Goddard Space Flight Center (Study Manager)
Martin H. Israel, Washington University (Chairman)
W. Vernon Jones, NASA Headquarters (Program Scientist)
Richard A. Mewaldt, California Institute of Technology (Chairman, Science and Facility Operations Subcommittee)
Dietrich Muller, The University of Chicago
Jonathan F. Ormes, NASA/Goddard Space Flight Center, (Project Scientist)
George F. Smoot III, University of California, Berkeley
Mark E. Wiedenbeck, The University of Chicago (Chairman, Instrumentation and Detector Development Subcommittee)

Foreign Participants:

Giulio Auriemma, University of Rome, ITALY
Giuseppi Basini, Laboratori Nazionali Frascati, ITALY
Per J. Carlson, University of Stockholm, SWEDEN
Philippe Goret, CEN-Saclay, FRANCE
Jun Nishimura, Institute of Space & Aeronautic Science, JAPAN
Ib L. Rasmussen, Danish Space Research Institute, DENMARK
Manfred Simon, University of Siegen, WEST GERMANY
Piero Spillantini, Laboratori Nazionali Frascati, ITALY
S. Alfred Stephens, Tata Institute for Fundamental Research, INDIA
Arnold W. Wolfendale, University of Durham, UNITED KINGDOM
Akira Yamamoto, National Laboratory for High Energy Physics, JAPAN

Subcommittee Members and Technical Advisors:

James H. Adams, Jr., Naval Research Laboratory
W. Robert Binns, Washington University, McDonnell Center for Space Science
Stephen Castles, NASA/Goddard Space Flight Center
Roger Dixon, Fermi National Accelerator Laboratory
Paul A. Evenson, Franklin Institute, University of Delaware
Michael A. Green, Lawrence Berkeley Laboratory
Robert Kephart, Fermi National Accelerator Laboratory
Peter Meyer, The University of Chicago
Ralph Nieman, Fermi National Accelerator Laboratory
Joe O'Connor, NASA/Goddard Space Flight Center
Donald V. Reames, NASA/Goddard Space Flight Center
Robert E. Streitmatter, NASA/Goddard Space Flight Center
James D. Sullivan, Massachusetts Institute of Technology
John P. Wefel, Louisiana State University

STOCHASTIC ACCELERATION IN THE TRANSRELATIVISTIC REGION AND PION PRODUCTION IN SOLAR FLARES

(in press, 20th International Cosmic Ray Conference)

James A. Miller[1] and Reuven Ramaty
NASA/Goddard Space Flight Center, Code 665
Greenbelt, MD 20771 USA

Ronald J. Murphy[2]
E.O. Hulbert Center for Space Research, Naval Research Laboratory,
Washington, DC 20375 USA

[1]also Department of Physics, University of Maryland, College Park, MD USA
[2]NAS/NRC Research Associate

ABSTRACT

The stochastic Fermi acceleration spectrum in the transrelativistic region obtained from a Monte-Carlo simulation for an energy-independent αT is much harder than the extension of the nonrelativistic analytic spectrum to this energy range for the same αT. The latter, with $\alpha T = 0.043$, was used to model the pion and nuclear line emissions for the impulsive phase of the 1982 June 3 flare, as well as the 2.223MeV emission from this flare. We find that the ratios of these three emissions for the Monte-Carlo spectrum with $\alpha T = 0.028$ are essentially the same as those for the analytical spectrum with $\alpha T = 0.043$. We also find that the acceleration time from ~30MeV to ~1GeV is $\lesssim$10s, consistent with the observations of the 1982 June 3 flare.

INTRODUCTION. We have carried out Monte-Carlo calculations of particle acceleration due to scattering by very massive hard spheres to simulate stochastic Fermi acceleration. Analytic expressions for the particle spectrum resulting from such acceleration are approximations valid only in the non- and ultra-relativistic regimes. We provide numerical results valid from the MeV to the GeV region and use these spectra to calculate the production of pions, neutrons, and nuclear lines in solar flares. We also study the acceleration times and compare our results with observations of the 1982 June 3 flare.

STOCHASTIC ACCELERATION. Processes in turbulent plasmas which cause particles to change their energy in a random way lead to stochastic acceleration /e.g., ref. 1/. When the energy changes are small compared to the particle energy, stochastic acceleration can be described as diffusion in momentum space. The particle energy spectrum can then be obtained by solving a diffusion equation which includes the particle sources and all applicable losses. For the diffusion coefficient derived /2,3/ for hard-sphere scattering with a constant scattering mean-free path λ, a steady source of q particles $cm^{-3}s^{-1}$ at injection energy E_0, escape from the acceleration region characterized by an energy-independent mean escape time T, and in the absence of any other losses, the steady-state particle energy spectrum for $E>E_0$ is given /4/ by

$$dN/dE = [6q/(p_0 c\alpha)]\cdot I_2(x_0)K_2(x) \quad (1)$$

in the nonrelativistic regime ($E<<mc^2$) and

$$dN/dE = [3q/(\alpha E_0(9 + 12/\alpha T)^{1/2})]\cdot(E/E_0)^{1/2-1/2(9+12/\alpha T)^{1/2}} \quad (2)$$

in the ultrarelativistic regime ($E_0>>mc^2$). Here, $\alpha=V^2/\lambda c$, where V is the velocity of the scatterers, $x=2(3pc/mc^2\alpha T)^{1/2}$, where p and m are particle momentum and mass, and K_2 and I_2 are modified Bessel functions. For both of these solutions, the combination of parameters αT characterizes the shape of the spectrum such that a larger value of αT corresponds to a harder spectrum. There is no analytic solution for the spectrum in the transrelativistic regime.

The nonrelativistic spectrum (1) has been used as the solar flare particle spectrum in calculations of nuclear reaction rates at the Sun /5/, implying $0.015 \lesssim \alpha T \lesssim 0.04$. In these calculations, however, equation (1) was extended into the transrelativistic region where it is not strictly valid. In particular, for pion production (threshold ~300 MeV/nucleon), the correct transrelativistic spectrum should be used. Equation (1) was also used to fit /6/ solar flare particle spectra observed in interplanetary space. We defer the comparison of these spectra with our numerical calculations to another publication.

METHOD OF CALCULATION. We performed a Monte-Carlo simulation of stochastic acceleration by modelling the interaction of particles with turbulence as scattering off an isotopic distribution of infinitely-massive hard spheres. We assume that all the scatterers have the same velocity $V = c\beta_S$, and that the scattering mean-free path λ is constant. We inject particles at an energy E_0, calculate the energy change in each collision, and allow each particle to escape after time t_{esc} which is selected uniformly for each particle from the interval $[0,t_{max}]$, where t_{max} is the maximum time a particle can be accelerated. We assume that the only particle loss is escape characterized by a constant mean escape time T and hence the probability for a particle to survive escape until t_{esc} is $P(t_{esc}) = \exp(-t_{esc}/T)$. Upon escape the particles are binned in energy with weight $P(t_{esc})$ to produce the escaping particle spectrum. We chose t_{max}/T to be large enough to ensure that the Monte-Carlo (numerical) spectrum corresponds to a steady-state solution of the diffusion equation. We employ particle splitting at certain energies in order to increase the efficiency of the calculation and obtain better statistics.

A particle-scatterer collision is simulated by selecting the laboratory system (LS) collision angle θ between the particle and a scatterer from the density function $f(\cos\theta) \propto \beta_r$, where $c\beta_r$ is the relative speed between the particle and scatterer. It is implicit in this function that both the scatterers and particles are isotropic. We take $\beta_S \ll 1$, in which case $f(\cos\theta) \propto |\vec{\beta}_S - \vec{\beta}|$, where $c\beta$ is the speed of the particle. In the rest frame of the scatterer, we take the collision to be isotropic and elastic, and so in this frame we select the scattering angles uniformly about the incident direction of the particle. Then given V, β, θ, and the scattering angles, we determine the scattered particle's energy in the LS by a kinematic transformation.

The probability of having undergone a collision in time Δt is $1-\exp(-\omega\Delta t)$, where ω is the collision frequency. It can be shown /7/ that the relativistically correct expression for ω is $c\gamma_r\beta_r/\lambda\gamma_S\gamma$. Here, the γ's are Lorentz factors corresponding to β_r, β_S, and β, and $\lambda = (n_S\sigma_0)^{-1}$ where n_S is LS density of scatterers and σ_0 is the hard-sphere rest-frame elastic scattering cross section. This definition of λ is identical to that used in the derivation /3/ of the momentum diffusion coefficient for hard-sphere scattering.

RESULTS. We have carried out calculations for $E_0 = 5$MeV, $T = 1$s, $t_{max} = 20$s, $\lambda = 1.5\times10^9$cm, and 2 values of V, 1.34×10^9cm/s and 1.16×10^9cm/s, leading to $\alpha T = 0.04$ and 0.03, respectively. These αT's are typical solar flare values, as is t_{max} if this time is identified with the total duration of the acceleration. A necessary condition for steady-state acceleration is $T \ll t_{max}$, which is the motivation for the choice of T. However, the V's and λ are much larger than expected solar flare values. In the flare acceleration region, V should be on the order of the Alfven velocity, ~10^8cm/s, and thus $\lambda \sim 10^7$cm for the above αT's. As long as the diffusion approximation (energy gain per collision < particle energy) is valid, the steady-state numerical spectrum depends only on αT and is independent of the specific values of V and λ. In the numerical calculation we took large values of V and λ in order to decrease the number of Monte-Carlo steps required to reach a given energy, and hence to decrease the computation time. For $V \sim 10^9$cm/s, the diffusion approximation is valid above ~10MeV/nucleon. We have also chosen a fairly high injection energy to decrease the computation time. The injection energy is not known, but it could be as low

as 5keV, an energy at which the proton velocity equals the scatterer velocity of 10^8cm/s.

The results are shown in Figs. 1 and 2. The upper curves at energies >10MeV are from the numerical calculations. In the nonrelativistic energy range 10--60MeV, we found that the numerical spectrum is well fit with the analytical spectrum $dN/dE \propto K_2(x)$, but at higher energies the numerical calculations diverge from K_2. (dN/dE is proportional to the escaping spectrum if T = constant.) We have continued the spectrum $\propto K_2$ to 1MeV, implicitly assuming that $V < 3\times10^8$cm/s (so that the diffusion approximation remains valid) and the injection energy <1MeV. The numerical spectra are normalized such that the integral of dN/dE above 30MeV is 1, while the K_2 have different normalizations since they were chosen to fit the numerical spectra between 10-60MeV.

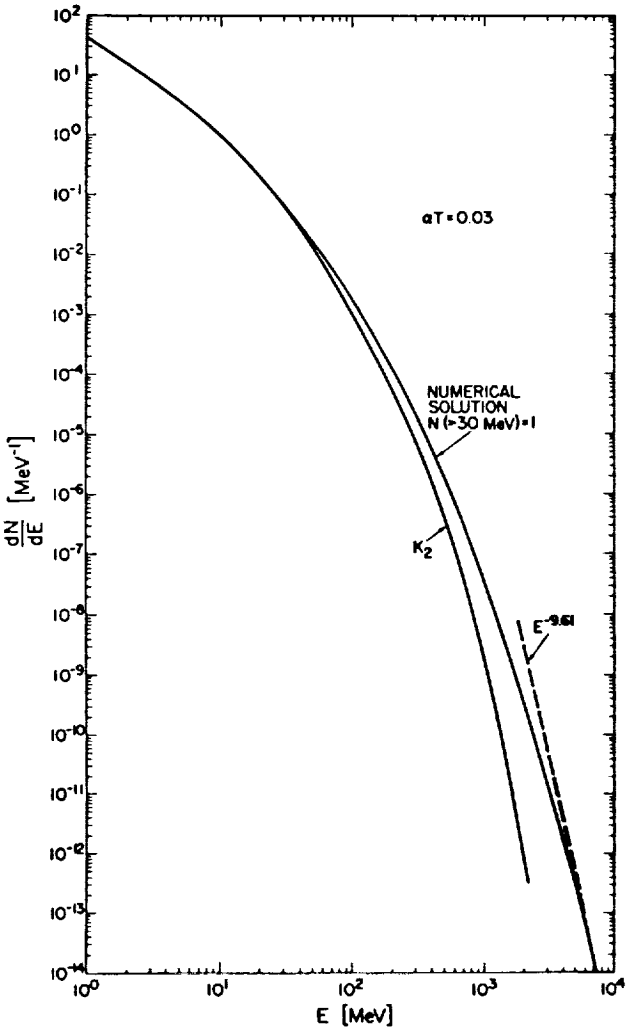

Fig. 1

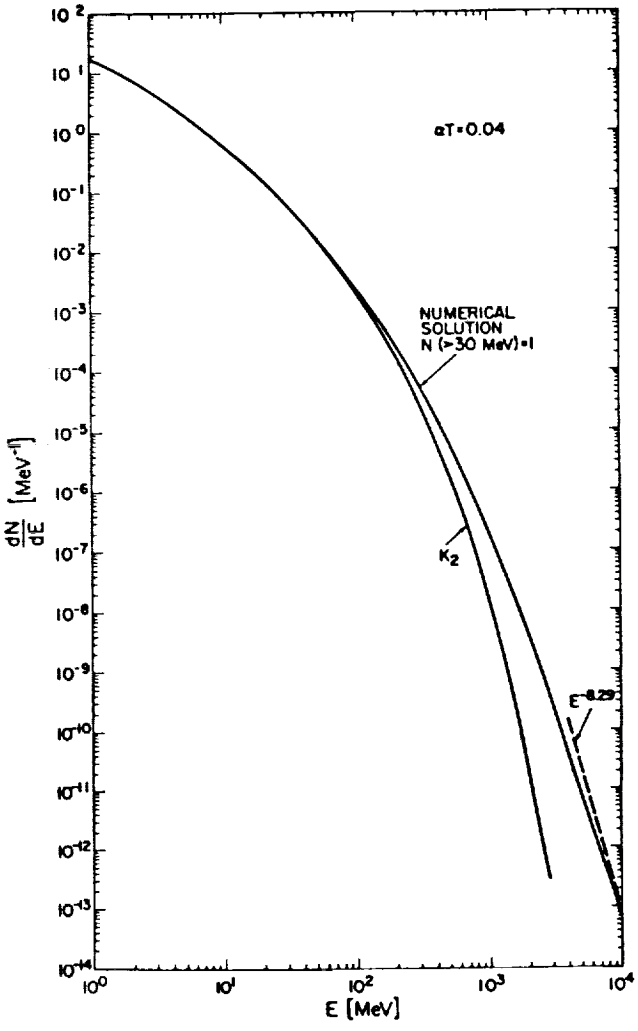

Fig. 2

[Numerical and nonrelativistic (K_2) stochastic acceleration spectra for αT = 0.04 and 0.03. The dashed curves are the unnormalized forms of the ultrarelativistic spectra from equation 2.]

We have also calculated the mean time required to accelerate particles from 5MeV/nucleon to various energies, which varies as α^{-1}. Since the V's and λ that we use in the numerical calculation yield the same α's as those expected in the actual flare acceleration region, the numerically calculated times should be representative of the actual flare acceleration time. We find that for $\alpha = 0.03s^{-1}$ the time required to accelerate particles from 5MeV/nucleon to 30, 400, and 6000MeV/nucleon is ~2, 6, and 16s, respectively. Thus, for t_{max} = 20s, the numerical spectrum for this α is the steady-state solution up to essentially 6GeV/nucleon.

Using the spectra shown in Figs. 1 and 2 and a similarly calculated spectrum for $\alpha T = 0.025$, we have calculated the thick-target yields of 100MeV photons from pions $dQ/d\epsilon(100MeV)$, neutrons Q_n, and 4.1-6.4MeV nuclear deexitation lines Q(4.1-6.4MeV), using the techniques of ref. /8/. The resultant yields, and the yields /8/ for the nonrelativistic spectra K_2, are given in Table 1. Here, both the numerical and analytic spectra are normalized to 1 proton above 30MeV. We see that for the harder numerical spectra the pion radiation yield increases by about an order of magnitude, the neutron yield by about a factor of 1.8, and the nuclear line yield by about 5-10%.

Table 1

αT	$10^7 dQ/d\epsilon(100MeV)$ [MeV^{-1}]		$10^4 Q(4.1\text{-}6.4MeV)$		$10^3 Q_n$	
	K_2	numerical	K_2	numerical	K_2	numerical
0.025	0.05	0.57	2.8	3.0	2.7	4.7
0.03	0.14	1.4	2.6	2.7	3.2	5.8
0.04	0.60	5.2	2.5	2.7	4.0	7.2

DISCUSSION. Pion radiation was observed so far only from the 1982 June 3 flare /9,10/. During the first emission peak (11:42:44-11:43:43 UT), the ratio of the pion emission to the nuclear line emission ($\sim 3.4\times10^{-4}$) was modelled /11/ using K_2 with $\alpha T = 0.043$. For the numerical spectra, we now deduce that $\alpha T = 0.028$ gives the same ratio. While this difference is significant, we find that $Q_n/Q(4.1\text{-}6.4MeV)$ is essentially the same for the numerical spectrum with $\alpha T = 0.028$ and K_2 with $\alpha T = 0.043$ (~19 in both cases). Thus, the conclusions of refs. /8/ and /11/ regarding the pion emission, 4.1-6.4MeV emission, and 2.2MeV line are not significantly altered. However, we have not yet evaluated the high-energy neutron spectrum for our new numerical results.

Observations /10,12/ show that at ~11:43.5 UT the 4.1-6.4MeV emission and the pion emission peaked simultaneously to within 16s, implying that the proton acceleration time from ~30MeV to 1GeV was less than this time. From the above results for $\alpha T = 0.03$, we estimate an acceleration time from 30MeV to 1GeV of ~10s consistent with the observations. For a fixed αT (determined from the shape of the spectrum) the acceleration time would be shorter if α were larger and T smaller. Leaving V unchanged (10^8cm/s), by decreasing λ from 10^7cm to 10^5cm (~ the gyroradius of a 1GeV proton in a 100G field), we would decrease the acceleration time to values as short as ~0.1s.

REFERENCES

1. Forman, M.A., Ramaty, R., and Zweibel, E.G. 1986, in Physics of the Sun ed. P.A. Sturrock (Dordrecht: Reidel), 2, p. 249.
2. Parker, E.N., and Tidman, D.A. 1958, Phys. Rev., 111, 1206.
3. Lee, M.A. 1978, private communication.
4. Ramaty, R. 1979, in Particle Acceleration Mechanisms in Astrophysics ed. J. Arons, C. Max, and C. McKee (New York: Am. Inst. Phys.), p. 135.
5. Murphy, R.J., and Ramaty, R. 1984, Adv. Space Res., 4, No. 7, p. 127.
6. McGuire,R.E.,and Von Rosenvinge,T.T. 1984, Adv. Space Res., 4, No. 2-3,117.
7. Landau, L.D., and Lifshitz, E.M. 1962, The Classical Theory of Fields (Oxford: Pergamon Press).
8. Murphy, R.J., Dermer, C.D., and Ramaty, R. 1987, Ap. J. (Suppl.), in press.
9. Forrest, D.J. et al. 1985, Proc. 19th Inter. Cosmic Ray Conf., 4, 146.
10. Forrest, D.J. et al. 1987, Adv. Space Res., in press.
11. Ramaty, R., Murphy, R.J., and Dermer, C.D. 1987, Ap. J. Lett., in press.
12. Chupp, E.L. et al. 1987, Ap. J., in press.

SH-2.2-2

SOLAR FLARE NUCLEAR GAMMA-RAYS AND INTERPLANETARY PROTON EVENTS

E.W. Cliver
Space Physics Div., Air Force Geophysics Lab., Hanscom AFB, MA 01731 USA

D.J. Forrest
Physics Dept., University of New Hampshire, Durham, NH 03824 USA

R.E. McGuire, T.T. von Rosenvinge, D.V. Reames, and H.V. Cane*
Lab. for High En. Astrophys., NASA Goddard SFC, Greenbelt, MD 20771 USA

S.R. Kane
Space Sciences Lab., University of California, Berkeley, CA 94720 USA

Abstract

We compared flare γ-ray line (GRL) events and solar energetic proton (SEP) events for the period from February 1980 - January 1985 and substantiated earlier results showing a lack of correlation between γ-ray-producing ions and interplanetary protons. This poor correlation results primarily from several large SEP events that originated in flares without detectable γ-ray emission. The converse case of GRL events unassociated with SEP events is rare. We present evidence which suggests that the ratio of trapped to escaping protons in GRL/SEP flares depends on the spatial scale size of the flare (cf., Cane et al., 1986; Bai, 1986). We affirm the result of Bai and Dennis (1985) that GRL flares are generally accompanied (75%) by metric Type II bursts.

1. Introduction. One of the more surprising results from the most recent solar maximum was the poor correlation observed between flare nuclear γ-ray fluences and the sizes of interplanetary proton events (Chambon et al., 1981; von Rosenvinge et al., 1981; Pesses et al., 1981; Cliver et al.,1983a; Yoshimori and Watanabe, 1985). This result is based on a relatively small number of events observed mainly during 1980-1981. The largest sample considered in any study to date was 16 events (Cliver et al., 1983a). In the present paper we compare γ-ray line (GRL) and solar energetic proton (SEP) events observed from February 1980 - January 1985 in order to substantiate this lack of correlation.

We also look for evidence that the time scale of a flare is an important parameter that might "order" the γ-ray/proton data as was recently indicated by Cane et al. (1986) and Bai (1986) (cf., Kocharov et al., 1983). Since SEPs are generally thought to be accelerated at coronal shocks, we determine the fraction of the γ-ray events during this period that were associated with metric Type II bursts to see if Type II shocks or their progenitors might be important for γ-ray-producing ions as well. Bai and Dennis (1985) and Bai (1986) have reported that Type II bursts were a characteristic feature of the GRL flares observed in 1980-1981.

2. Data Analysis.

2.1 Peak ~ 10 MeV Proton Fluxes vs. 4-8 MeV Gamma-Ray Line Fluences. The proton data are from the NASA GSFC experiments on IMP-8 and ISEE-3. For three events we used the Helios particle data published by McDonald and Van Hollebeke (1985) and McDonald et al. (1985). We identified a total of 66 prompt proton events with $J(>20\ MeV) > 10^{-3}$ pr cm^{-2} s^{-1} sr^{-1} MeV^{-1} for which we were able to make confident visible disk flare associations. The 4-8 MeV GRL fluences (or upper limits) were either measured directly by the UNH/NRL/MPI Gamma Ray Spectrometer on SMM or were inferred from hard X-ray observations from the U Cal/

*Also: Dept. Of Phys. & Astronomy, Univ. of Maryland, College Park, MD 20742 USA

Berkeley experiment on ISEE-3 by making use of the relationship between the 4-8 MeV fluence and the >300 keV electron bremsstrahlung continuum flux (Forrest, 1983). Of the 66 proton events, 50 originated in western hemisphere flares. For 45 of these well-connected flares, γ-ray (hard X-ray) observations were available from either SMM or ISEE. These 45 events are plotted in Fig. 1 along with three well-connected GRL events that were associated with small ($J(>20) < 10^{-3}$) SEP events or lacked SEP association. As we had shown previously with fewer events, the γ-ray-producing and interplanetary ions do not appear to be closely related. We note that the largest GRL events (>10 γ cm^{-2}) are generally accompanied by significant SEP production. Conversely, there are seven large ($\geq 4 \times 10^{-1}$) SEP events that lacked detectable > 300 keV emission. These seven events (23 Nov 80, 30 Mar 81, 10 May 81, 20 Jul 81, 05 Dec 81, 09 Dec 81, 19 Dec 82) are characterized by gradual 1-8 Å decay rates, weak (S_p(9 GHz) $\lesssim$ 100 sfu) to moderate (S_p(9 GHz) ~ 500 sfu) impulsive phases, and associations with metric and/or kilometric Type II bursts (6/7) (Kahler et al., 1978; Cliver et al., 1983b; Cane and Stone, 1984).

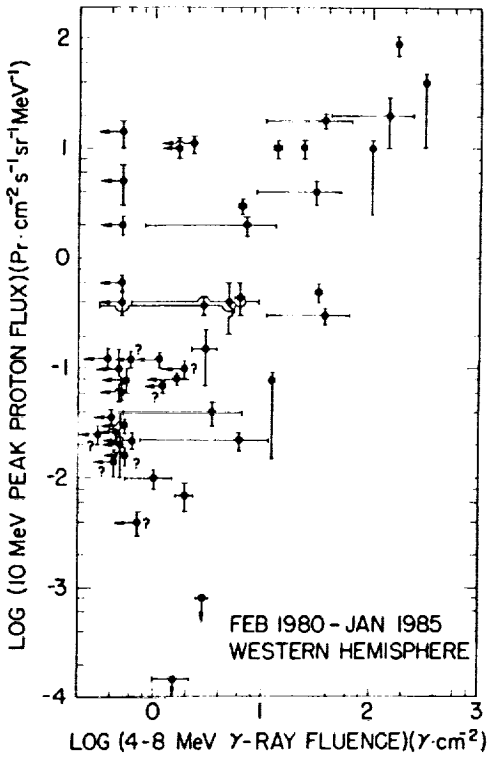

Fig. 1. Peak ~ 10 MeV Proton Flux vs. 4-8 MeV GRL fluence.

2.2 The Ratio of γ-Ray-Producing Ions to Interplanetary Protons vs. the Soft X-ray Decay Rate. For a sample of 10 GRL/SEP flares, not all of which were well-connected, Bai (1986) showed that the ratio of the number of γ-ray producing protons to the number of interplanetary protons varies greatly from event to event but that, on average, impulsive flares have a higher ratio than gradual flares. Since Pallavicini et al. (1977) have associated impulsive soft X-ray flares with low-lying (< 10^4 km) sources and gradual events with extended (~ 5 x 10^4 km) structures, Bai's result suggests that the probability of proton escape is dependent on the scale size (loop height) of the flaring region (cf., Cane et al., 1986). To test this result, we have plotted in Fig. 2 the ratio R (= (4-8 MeV GRL fluence / 9-23 MeV peak proton flux)) vs. τ, the e-folding time of the flare associated soft X-ray burst for the events in Fig. 1. We measured τ from the peak of the GOES 1-8 Å profile. For a given flare, R is proportional to the ratio, near 10 MeV, of the number of γ-ray-producing (trapped) ions to the number of interplanetary (escaping) protons. Despite the uncertainties, the data in Fig.

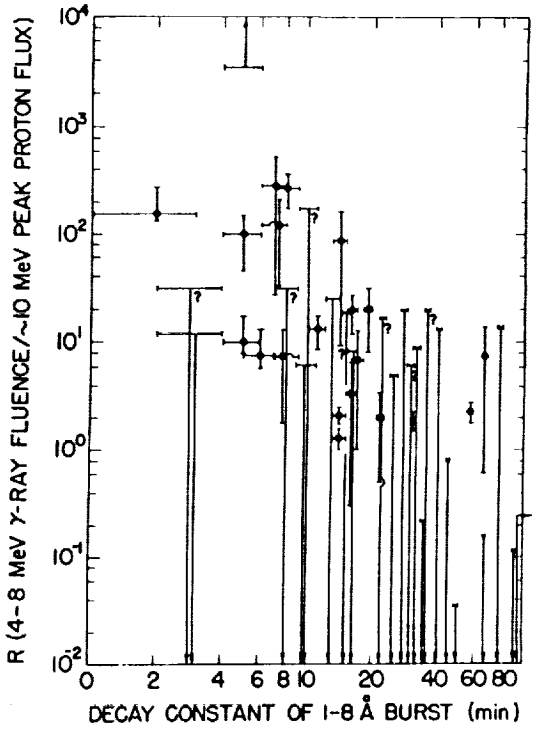

Fig 2. Ratio of GRL to SEP Protons vs. Soft X-ray Decay Rate.

2 display an apparent trend. If we take the limiting values of R to be the actual values for the events with upper (or lower) limits, then the median value of R for the 14 most impulsive events ($\tau \leq 10$) is 66, compared to R = 11 for the 16 intermediate ($10 < \tau \leq 30$) events and R = 2 for the 13 most gradual ($\tau > 30$) events. We also determined the R values of the 16 eastern hemisphere SEP events in our sample and found them to be, for the most part, consistent with the above trend, after taking the propagation effect into account. There are three eastern hemisphere events, however, with τ values ~ 20 minutes that have lower than expected R values. The data for these events are as follows: 30 Jan 1982, E13°, $R = 2.4 \pm 2.1 \times 10^{-2}$; 04 Sep 1982, E38°, $R < 1.7 \times 10^{-1}$; 25 Dec 1982, E45°, $R < 8.3 \times 10^{-1}$. Presumably R would be even smaller if these events had been well-connected. The 30 Jan and 04 Sep flares were associated with interplanetary Type II bursts (Cane, 1985) and the 25 Dec flare was followed within 48 hours by a sudden commencement at Earth (Cane et al., 1986).

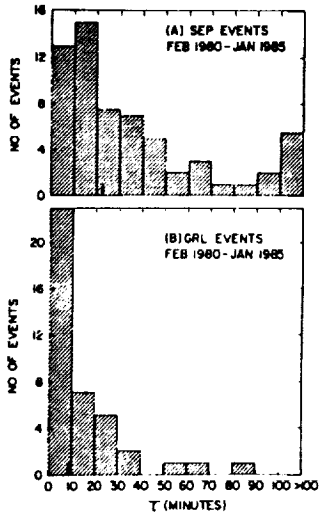

Fig. 3. Histograms of τ.

Cane et al. (1986) separated interplanetary electron events into two classes on the basis of the time scale of the soft X-ray emission of the associated flares. Similarly, from a consideration of hard X-ray ray burst time profiles, Bai (1986) argued for two distinct classes of GRL/SEP flares. Events with $\tau \leq 10$ minutes correspond to the class of impulsive events of Cane et al., while those with $\tau > 10$ minutes approximate their gradual events. There is no indication of a sharp division between the events in Figure 2 near $\tau = 10$. Nor is there evidence for bimodality in the histograms of τ for either SEP or GRL (2σ) events (Fig. 3). The lack of evidence for two classes of events in either Figures 2 or 3 may be due to "mixed" events in which both acceleration processes are operating. The two distributions in Fig. 3 are not mutually exclusive; there are 17 common events. The GRL events are more impulsive, with a median τ value of 9 minutes compared to 22.5 minutes for the SEP events. Detectable (2σ) GRL events with τ values > 30 minutes are rare.

2.3 Type II Bursts and Gamma-Ray Line events. Through January 1985, ~ 150 γ-ray continuum events were observed by SMM; 45 of these had 4-8 MeV line emission at the 2σ level. The Type II burst associations for the continuum and line events are shown in Table 1. In 1(A) it can be seen that the relatively high degree of association found by Bai and Dennis (1985) for GRL events from 1980-81 persists for the larger sample. In Table 1(A) we considered only reports of metric Type II in SGD by Culgoora, Weissenau, and Fort Davis. Relaxing these criteria in 1(B) to include such events as metric Type IVs, possible Type IIs, or unclassified activity, in addition to reports of Type II or Type II-like activity by other observatories, increases the percentage of IIs without 2σ lines. The distributions in Table 1 may be a consequence of the Big Flare Syndrome (Kahler, 1982); in Table 1(B) the median >300 keV fluence of the 74 events with Type II or possible Type II emission is 31 γ cm^{-2}, compared to 4.5 γ cm^{-2} for the 70 events that lacked Type II association. Alternatively, the presence of an additional, Type II - related, acceleration mechanism could be the cause

		γ-Ray Events (>300 keV)	
		> 2σ (4-8 MeV)	< 2σ (4-8 MeV)
(A) Type II	Yes	32	20
	No	10	73
		> 2σ (4-8 MeV)	< 2σ (4-8 MeV)
(B) Type II	Yes	37	37
	No	8	62

Table 1.

of the larger γ-ray fluences observed in the events with associated Type II bursts. For 28 of the 33 2σ 4-8 MeV GRL events that had associated Type II bursts, the Type II began within six minutes after the onset of the γ-ray emission. A disturbance propagating from the low corona at a characteristic speed of 1000 km s^{-1} will reach the 100 MHz plasma level (a typical Type II starting frequency) in a 10 x Baumbach-Allen atmosphere within approximately six minutes. We note that the line emission in the eight GRL events that lacked any evidence for Type II emission tended to be weak; only one of these eight events had a 2.2 MeV fluence at the > 2σ level.

3. Discussion. The poor correlation between γ-ray-producing ions and interplanetary protons is caused primarily by a number (seven) of large SEP events from flares that lacked detectable γ-ray emission. The absence of strong impulsive phases in these events, coupled with the fact that 6 of the 7 events had associated coronal and/or interplanetary Type II bursts, argues that the protons observed in space following these flares resulted from shock acceleration (cf., Cliver et al., 1983b). The persistent high degree of association between Type II bursts and GRL events leads us to question if the Type II shock or its progenitor, i.e., the low coronal propagating disturbance eventually observed as a Type II burst, might play an important role in accelerating the bulk of the impulsive phase γ-ray-producing ions as well. The Type II shock is a common thread linking the SEP and GRL flares considered in this study. Approximately 75% of the events in each sample had associated Type IIs. We speculate that in impulsive events shock acceleration begins low in the corona where energetic ions are trapped on closed loops while in gradual flares this "second phase" acceleration occurs primarily in the high corona where the protons have greater access to open field lines. This picture is appealing because of its simplicity but significant questions remain concerning the speed of shock formation and subsequent acceleration (Ellison and Ramaty, 1985; Decker and Vlahos, 1985), the cause of the variation of e/p ratios (Evenson et al., 1984) and electron spectra (Evenson et al., 1985) with τ, and the nature of the recently discovered delayed, or extended, pion emission observed in the 03 June 1982 neutron flare (Forrest et al., 1985; Murphy et al., 1987).

References

Bai, T., 1986, Astrophys. J., 308, 912.
Bai, T., and B.R. Dennis, 1985, Astrophys. J., 292, 699.
Cane, H.V., 1985, J. Geophys. Res., 90, 191.
Cane, H.V., et al., 1986, Astrophys. J., 301, 448.
Cane, H.V., and R.G. Stone, 1984, Astrophys. J., 282, 339.
Chambon, G., et al., 1981, Solar Phys., 69, 147.
Cliver, E.W., et al., 1983a, Proc. 18th ICRC, 10, 342.
Cliver, E.W., et al., 1983b, Astrophys. J., 264, 699.
Decker, R.B., and L. Vlahos, 1985, Proc. 19th ICRC, 4, 10.
Ellison, D.C., and R. Ramaty, 1985, Proc. 19th ICRC, 4, 6.
Evenson, P., et al., 1984, Astrophys. J., 283, 439.
Evenson, P., et al., 1985, Proc. 19th ICRC, 4, 74.
Forrest, D.J., 1983, AIP Conf. 101 Proc., p. 3.
Forrest, D.J., et al., 1985, Proc. 19th ICRC, 4, 146.
Kahler, S.W., 1982, J. Geophys. Res., 87, 3439.
Kahler, S.W., et al., 1978, Solar Phys., 57, 429.
Kocharov, G.E., et al., 1983, Proc. 18th ICRC, 4, 105.
McDonald, F.B., and M.A.I. Van Hollebeke, 1985, Astrophys. J. Lett., 290, L67.
McDonald, F.B., et al., 1985, Proc. 19th ICRC, 4, 98.
Murphy, R., et al., 1987, Astrophys. J. Suppl. Ser., 63 (in press).
Pallavicini, R., et al., 1977, Astrophys. J., 216, 108.
Pesses, M.E., et al., 1981, Proc. 17th ICRC, 3, 336.
von Rosenvinge, T.T., et al., 1981, Proc. 17th ICRC, 3, 28.
Yoshimori, M., and H. Watanabe, 1985, Proc. 19th ICRC, 4, 90.

SOLAR ENERGETIC PROTON EVENTS AND CORONAL MASS EJECTIONS NEAR SOLAR MINIMUM

S.W. Kahler

Emmanuel College, Boston, Massachusetts 02115 USA

E.W. Cliver

Air Force Geophysics Laboratory, Hanscom AFB, Massachusetts 01731 USA

H.V. Cane, R.E. McGuire, and D.V. Reames

Laboratory for High Energy Astrophysics, Goddard Space Flight Center, Greenbelt, Maryland 20771 USA

N.R. Sheeley, Jr., and R.A. Howard

Naval Research Laboratory, Washington, D.C. 20375 USA

Abstract

We have examined the association of coronal mass ejections (CMEs) with solar energetic (9-23 MeV) proton (SEP) events during the 1983-1985 approach to solar minimum. Twenty-two of 25 SEP events were associated with CMEs, a result comparable to that previously found for the period 1979-1982 around solar maximum by Kahler et al. (1984a). Peak SEP fluxes were correlated with CME speeds but not with CME angular sizes. In addition, many associated CMEs lay well out of the ecliptic plane. In a reverse study using all west hemisphere CMEs of speeds exceeding 800 $km \cdot s^{-1}$ and covering the period 1979-1985, we found that 29 of 31 events originating on the solar disk or limb were associated with observed SEPs. However, in contrast to the previous study, we found no cases of SEP events associated with magnetically well connected flares of short duration that lacked CMEs.

1. Introduction. The solar origin of solar energetic proton (SEP) events remains an important problem. Kahler et al. (1983; 1984a) compared SEP events observed during 1979-1982 by the GSFC detectors on the IMP-8 and ISEE-3 spacecraft with coronal mass ejections (CMEs) observed by the NRL Solwind coronagraph. A CME association was found for 26 of the 27 SEP events associated with Hα flares. These CMEs were generally large loop or fan-shaped structures with high ($v > 500$ $km \cdot s^{-1}$) speeds. A correlation of peak 4-22 MeV fluxes with both CME speeds and angular sizes was found. Two basic models have been proposed to explain the close association between SEP events and CMEs (Kahler et al., 1984a). One is that the CME provides an open coronal magnetic field configuration, allowing escape of SEPs. Another is that the CME drives a shock which accelerates the protons.

A sharp drop in the rate of occurrence of CMEs during 1984-1985 has been reported (Howard et al., 1986; Hundhausen, 1987). The average speed and angular size of Solwind CMEs observed during 1984-1985 are only about half those observed for 1979-1981. This change reflects a reduction in the relative number of the kind of large, bright CMEs that were associated with SEPs during

*Also: University of Maryland, College Park, Maryland 20742 USA

1979-1982. As a result, we can test under new conditions the correlation of SEP events and CMEs found in the 1979-1982 period.

2. Analysis. We used energetic proton data from the GSFC experiments on the IMP-8 and ISEE-3 spacecraft to select 29 SEP events during the years 1983 to 1985. Only those SEP events that appeared to arise from solar flare events were used. Velocity dispersion and accompanying relativistic electron events were used in the selection process. The smallest 9-23 MeV proton fluxes detectable above background were about 5×10^{-3} p$(cm^2 \cdot sr \cdot s \cdot MeV)^{-1}$. Observations by the NRL Solwind coronagraph were available for the periods preceding the onsets of 25 events. Twenty-two of the 25 events were accompanied by observed CMEs. Speeds were determined for 19 events, and these ranged from 400 $km \cdot s^{-1}$ to 1440 $km \cdot s^{-1}$. The logs of the peak 9-23 MeV proton fluxes correlate ($r = 0.51$) with the speeds at the 96% confidence level, as shown in Figure 1. The slope of the least squares best fit is nearly identical to that of the similar plot in Kahler et al. (1984a) for 4-22 MeV protons, but the fit of Figure 1 is lower than that of Kahler et al. by a factor of 10 in peak flux. The difference in energy ranges of the protons accounts for all but about a factor of 2 of this difference. The two CMEs associated with flares within 45° of central meridian appear in the upper left hand corner of the plot, suggesting that their projected speeds are underestimated. In contrast to Kahler et al., we find no correlation ($r = -0.09$) between the logs of the peak 9-23 MeV proton fluxes and the angular sizes of the associated CMEs.

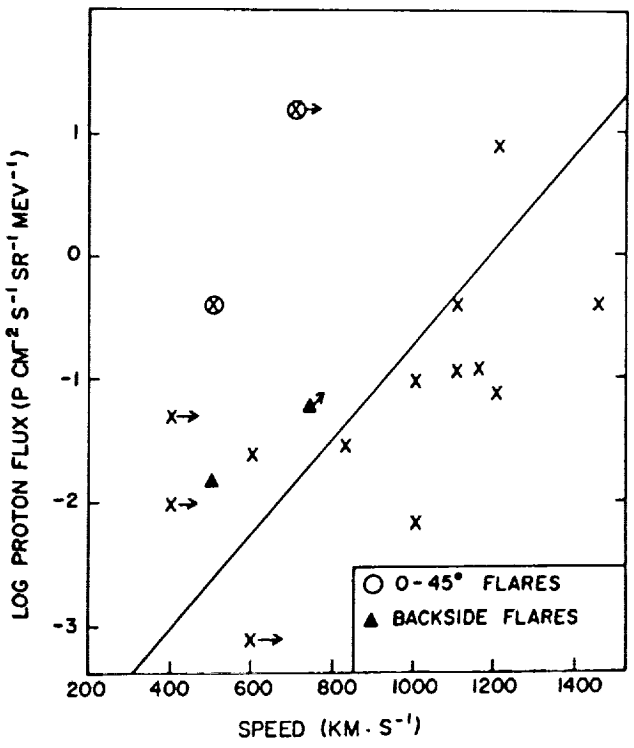

Figure 1. Logs of the peak 9-23 MeV proton fluxes plotted against the speeds of the associated CMEs. Speeds are measured in the plane of the sky. Arrows indicate lower limits. The least squares best fit is log $F = 3.88 \times 10^{-3}$ v $(km \cdot s^{-1}) - 4.56$.

We have examined the three cases of SEP events with no associated CMEs. In two cases, on 11 May and 12 May 1983, flares occurred at E 24° and E 15° in region 4171. CMEs from flares this close to central meridian are generally difficult to observe (Kahler et al., 1984b). The third flare, at E 45° on 25 April 1984, was the large γ-ray flare that gave rise to a neutron decay event (Evenson et al., 1985). The X13 X-ray burst showed a long duration enhancement (LDE) of > 10 hr and on that basis would be expected to result in a CME (Sheeley et al., 1982). Observations 2 hr after the peak of the flare showed no apparent CME, although an artifact in the data compromised the observation somewhat. We conclude that

none of the 25 SEP events is clearly not associated with a CME. We did not find any further examples of the four SEP events of Kahler et al. (1984a) associated with short duration X-ray events at magnetically well connected solar sites but without associated CMEs.

As a second part of the analysis we began with a list of all west hemisphere CMEs with speeds of $v > 800$ km$\cdot$s^{-1} and asked how many of these CMEs were associated with 9-23 MeV proton events. We included all such events from 1979 to 1985. Any events for which we could find an associated 1-8 Å X-ray event were considered to be frontside (disk) events; others were considered backside events. CMEs for which no SEP event was seen were considered null events only if the background 9-23 MeV proton flux did not exceed 10^{-2} p(cm$^2\cdot$sr$\cdot$s$\cdot$MeV)$^{-1}$. The results are shown in Table 1. The number of frontside events (31) was more than twice the number of backside events (13). This ratio can be understood if we assume that (1) all the fast CMEs are within 45° of the limb and (2) the associated X-ray events, typically LDEs of $\sim 10^5$ km height (Kahler, 1977), can be seen only at longitudes of $< 105°$, corresponding to occultation heights of $< 25{,}000$ km. In this case the longitude range of the frontside events is 60° and that of the backside events is 30°.

Only 2 of the 31 frontside fast CMEs were not associated with SEP events. Neither of these CMEs, on 5 April 1982 and 1 May 1983, lay in the ecliptic, and neither was associated with a reported metric type II burst, one of the best signatures of SEP events (Cliver et al., 1985). The logs of the peak 9-23 MeV fluxes of the 33 proton events of Table 1 correlate with the CME speeds at the 85% confidence level ($r = 0.27$), again producing a best fit slope nearly identical to that of Figure 1. We also find no correlation ($r = 0.10$) between the logs of the peak 9-23 MeV fluxes and the angular sizes of the 33 CMEs. Eleven of the 33 CMEs lay out of the ecliptic with 5 at least 45° away from the ecliptic.

Table 1. Association of 9-23 MeV SEP Events with $v > 800$ km$\cdot$s^{-1}.

	Protons	No Protons
Frontside	29	2
Backside	4	9

3. Conclusions. The principal result of this study is that the finding of Kahler et al. (1984a) that nearly all SEP events are associated with fast, large CMEs can now be extended to the period approaching solar minimum. The significant change in the average characteristics of CMEs during the 1984-1985 period has made no obvious difference to the relationship between SEP events and CMEs. We have found that for 4 backside SEP events of Table 1 the CME was the only observed solar signature. As in Kahler et al., we found a correlation between peak proton fluxes and CME speeds, and we find that nearly all fast ($v > 800$ km$\cdot$s^{-1}) CMEs are associated with the production of $E > 10$ MeV protons. A significant fraction ($\sim 1/3$) of the CMEs associated with SEP events lie out of the ecliptic.

Our results differ in two significant ways from those of Kahler et al. We did not find a correlation between logs of peak proton fluxes and CME angular sizes. This fact and the result that many associated CMEs lay out of the ecliptic suggest that the geometry of CMEs may not be important for SEPs.

However, most CMEs associated with SEPs come from the relatively small populations of loop, fan, halo, and complex CMEs, rather than from the more numerous spike and streamer blowout classes (Howard et al., 1985, 1986). Another difference from Kahler et al. was that we found no further examples of the SEP events associated with magnetically well connected, short-duration X-ray flares. These SEP events, unaccompanied by CMEs, now appear to be only a small fraction (< 10 %) of all observed E > 10 MeV SEP events.

4. Acknowledgements. This work was supported at Emmanuel College by AFGL Contract AF 19628-82 0039, at NRL by NASA DPR W 14, 429, and at GSFC/University of Maryland by NASA grant NGR 21-002316.

References

Cliver, E.W., et al. 1985, J. Geophys. Res., 90, 6251.
Evenson, P., et al. 1985, Proc. 19th ICRC, 4, 130.
Howard, R.A., et al. 1985, J. Geophys. Res., 90, 8173.
Howard, R.A., et al. 1986, in The Sun and the Heliosphere in Three Dimensions, ed. R.G. Marsden (Dordrecht: D. Reidel), p.107.
Hundhausen, A.J., 1987, J. Geophys. Res., submitted.
Kahler, S. 1977, Astrophys. J., 214, 891.
Kahler, S.W., et al. 1983, Proc. 18th ICRC, 4, 6.
Kahler, S.W., et al. 1984a, J. Geophys. Res., 89, 9683.
Kahler, S., et al. 1984b, Solar Phys., 93, 133.
Sheeley, N.R., Jr., et al. 1983, Astrophys. J., 272, 349.

SH-4.2-6

ON THE SOURCES OF SOLAR ENERGETIC PARTICLES

H. V. Cane, D. V. Reames and T. T. von Rosenvinge
Laboratory for High Energy Astrophysics
NASA/GSFC, Greenbelt, MD 20771, USA

Abstract

We have examined the time histories of energetic (>1 MeV) particles as detected by instruments in the earth's neighbourhood over an 18 year period commencing mid-1967. The majority (>75%) of the events extending to proton energies above 20 MeV have their origins in a flare event which includes H-alpha emission, soft X-rays and metric radio bursts of type II and/or type IV. We have assembled a list of 241 events for which the sources are thus well identified. Two further particle increases have been associated with non-flare events. Of the 82 events originating in regions to the east of central meridian, the sources of 68 (83%) were sufficiently energetic that they also generated interplanetary shocks detected at earth. We suggest that shocks are responsible for particles being detectable from source regions not magnetically connected to earth.

1. Introduction. Two major characteristics of solar energetic particle events can be explained by the acceleration of particles at shocks. Coronal shocks can account for the prompt acceleration of particles onto magnetic field lines which are far removed from the flare site. Interplanetary shocks can account for the large delays to maximum intensity for many events. The time structure of solar proton events as a function of viewing angle and energy is determined by the relative contribution of particles from coronal and interplanetary shocks. A two component structure of solar proton events has previously been suggested /1/,/2/ although in the former paper the proposal was not given a physical interppetation. In this paper we are primarily concerned with the component attributed to acceleration at interplanetary shocks. We show that particle fluxes at an energy of about 2 MeV, measured near shock passage, are correlated with the average shock strength.

2. Data and results. We have assembled a list of 301 proton increases with a flux above 3 x 10-3 particles.cm-2.ster-1.sec-1.MeV-1 in the energy range 9-23 MeV which occurred during the period late May 1967 to July 1985. The source of data was Goddard Space Flight Center experiments on IMPs -4,-5,-7,-8 and ISEE-3. Where possible each event was associated with a source. For the majority of the events there was a well defined soft X-ray increase and metric radio bursts of type II and/or type IV at the time of an H-alpha flare, all of which occurred close to the onset of the more energetic particles. Almost all the identifications are the same as those published previously e.g. /3/.The majority of the events not assigned a source probably originated from beyond the western solar limb. We estimate that such events

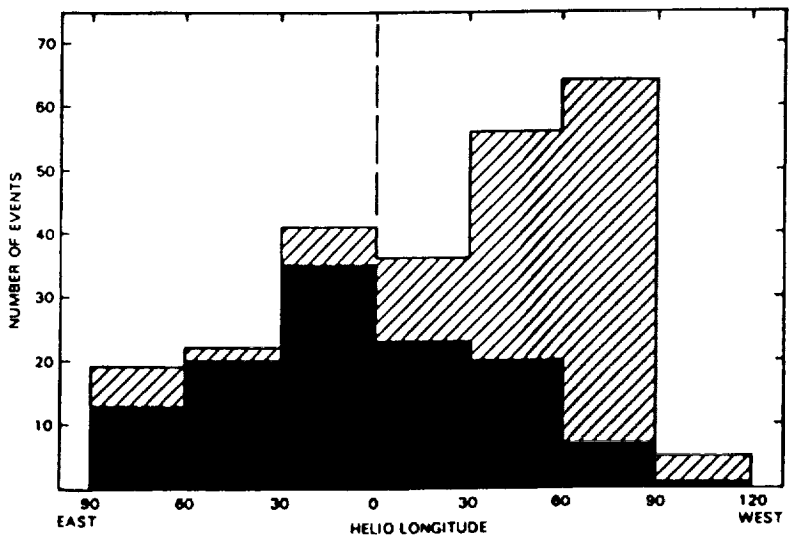

Figure 1.

represent about 15% of all events extending above 20 MeV. We estimate that slightly less than 1% of all > 20 MeV events have their origins in a non-flare event on the solar disk. Two events out of a final list of 243 events with identified sources, have been identified with disappearing filaments outside active regions /4/. About 30% of the original list of proton increases was excluded on the basis of missing solar data.

Figure 1 shows the distribution of the 243 events as a function of the heliolongitude of the source region. Whereas almost half the events originate in regions between W30 and W120 a significant number originate in regions to the east of central meridian. We argue that these eastern events are detectable at earth only because of the presence of strong interplanetary shocks. The black section of figure 1 shows the fraction of the solar events that also generated shocks that were detected at or near the earth. For a number of the other eastern solar events we know that there was a strong shock because of the detection of interplanetary type II radio emission (/5/) but the shock did not extend far enough in longitude to intercept the earth.

Figure 2 shows time profiles at three energies of three events which originated in different heliolongitudes. The times of the flares are indicated. Each event was associated with a strong interplanetary shock whose time of passage at the spacecraft is indicated with a dashed line. In each event the lowest energy channel (~7 MeV) peaks near shock passage and the peak fluxes are about the same. The highest energy channels (~140 MeV) are very different. The July 1980 event shows no increase. The November 1982 event shows the classic profile of a well connected event. The profiles for the middle energy channels (~30 MeV) are not significantly different from the 7 MeV channel. However the profile for the November 1982 event is very important. It displays the 'textbook' profile of an Energetic Storm Particle event i.e. a shock-associated enhancement super-imposed on the classic profile of a well connected prompt particle event. We note that such profiles are rare, particularly at 30 MeV. However this profile has the obvious interpretation that the event has two components and if the nine profiles of figure 2 are viewed in this context one can see a gradual change with connection longitude and energy. For each of the three events the low energy particles peak near shock passage. For the poorly connected event the higher energy particles also peak near the shock. A solar component is only well defined for the higher energy channels for the best connected event.

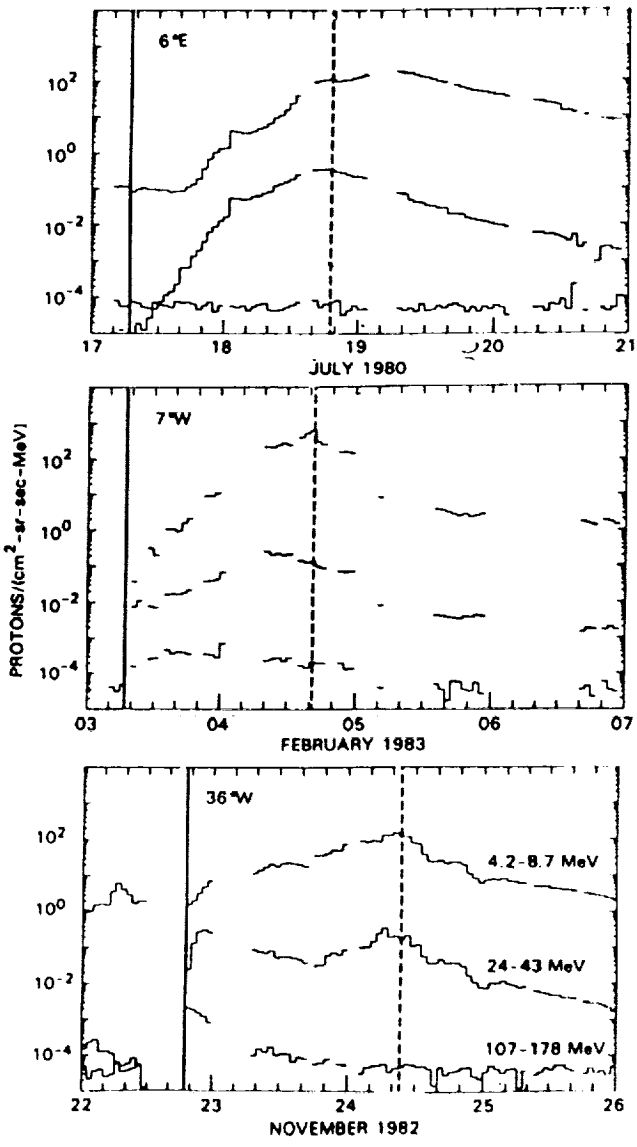

Figure 2.

For all 243 events of our study similar characteristics prevail. Moreover the same pattern emerges when individual events are viewed from widely spaced locations using multiple spacecraft. Differences between events can be attributed to shocks of

differing strengths.

Figure 3 illustrates the important role played by the interplanetary shocks. For all events for which there was an interplanetary shock we measured the peak flux in the ~2 MeV range. For events which were well connected an estimate of the flux due to the prompt component was subtracted. Figure 3 shows these peak fluxes as a function of the transit speed of the associated shock. This speed is deduced from the time it takes the shock to transit from the sun to 1 AU and is a good estimate of an average strength of the shock. It is clear that the peak fluxes are correlated with the shock speeds, consistent with the shocks accelerating these particles.

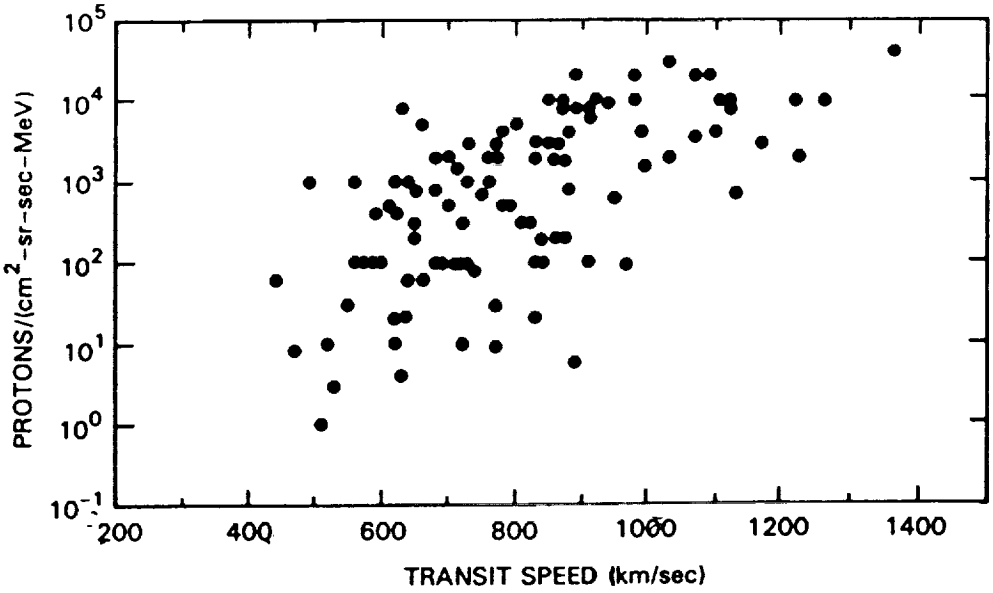

Figure 3.

We have investigated how the shock component varies as a function of the heliolongitude of the source region. Since the strongest shocks originate near central meridian, the largest particle increases are associated with central meridian solar events too. One anticipates that such shocks will be quasi-parallel. Our interpretation of the role of shocks in generating the observed particle profiles eliminates the need for the ad hoc mechanism of 'coronal diffusion' in understanding the azimuthal distribution of solar particles.

3. Summary. Interplanetary shocks play a major role in solar energetic particle events. We believe that all eastern solar events which produce particles detectable at earth, also generate interplanetary shocks. In most cases these shocks are detected at earth. We show that the peak fluxes in the vicinity of the shocks are correlated with estimates of the shock strengths, consistent with acceleration of the particles by the shocks.

4. Acknowledgements. This work was supported in part by NASA grant NGR 21-002-316.

References

1. McKibben, R.B.: 1972, J. Geophys. Res., 77, 3957.
2. Evenson, P. et al.: 1982, J. Geophys. Res., 87, 625.
3. Van Hollebeke, M.A.I. et al.:1975, Solar Phys., 41, 189.
4. Cane, H.V. et al.: 1986, J.Geophys. Res., 91, 1.
5. Cane, H.V.: 1985, J. Geophys. Res., 90, 191.

ENERGETICS OF THE SHOCK POTENTIAL

Frank C. Jones
Donald C. Ellison*
NASA/Goddard Space Flight Center, Code 665
Greenbelt, MD USA

*also Astronomy Program
University of Maryland
College Park, MD USA

1 Introduction. The theory of acceleration of charged particles by plasma shocks has been highly developed in the last few years. However, most theories to date treat the shock itself as a given structure in a plasma and consider the accelerated particles as a separate population, different from those of the background plasma that support the shock. The only work that has tried to treat all particles on an equal footing and thereby describe the injection process as well as the acceleration have been Monte Carlo simulations [Ellison et al., 1981; 1983] that have shown that the accelerated particles arise naturally from the thermal particles that make up the shock itself. These simulations also include the dynamic effect of the accelerated particles on the structure of the shock.

One difficulty with this approach, however, is that the efficiency with which the shock injects thermal particle into the acceleration process can depend in a sensitive manner on the details of the shock interface, and in particular, on the presence of an electrostatic potential jump at the shock. Furthermore, since such a potential jump can effect particles with different charge to mass ratios differently, it can have a strong influence on the predicted abundance ratios of the accelerated particles. It is clear that the shock structure must be understood before reliable calculations of particle injection are obtained.

It has been pointed out by Goodrich and Scudder [1984] (GS) that the detailed structure of the magnetic field in a shock layer can explain the observation that while the ions passing through a shock potential jump lose an amount of energy comparable to their flow, energy the electrons never gain more than ~50 eV [Formisano, 1982; Greenstadt et al., 1980; Ogilvie et al., 1982]. They point out that while the ions are unmagnetized on the scale of the shock and will go straight through the electrons are fully magnetized and will be deflected such that they lose energy in the transverse electric field produced by the plasma flow. This field is given by $\vec{E}_m = -\vec{V} \times \vec{B}/c$ and electrons obtaining a component of velocity parallel to $\vec{E}_m$ give up energy to the field. GS go on to argue that an excursion of the magnetic field out of the plane defined by the asymptotic magnetic field and the shock normal (the coplanarity plane) would produce this electron velocity.

It is the purpose of this paper to show that the difference between proton energy loss and electron energy gain can be understood from a knowledge of the asymptotic properties of the shock that are derivable from the Rankine-Hugoniot relations. No

reference to a component of the magnetic field that is out of the coplanarity plane is required. At the same time we show that such a field does exist and calculate its magnitude.

2 Calculation. If the energy gained by electrons in passing through the potential jump is not equal to the energy lost by the ions, a net transfer of energy from the plasma to the electromagnetic field occurs. This energy transfer is $\vec{E}\cdot\vec{j}$ where $\vec{E}$ is the electric field and $\vec{j}$ is the current density. Since by charge neutrality there is no net current through the shock the electric field of the potential jump can do no net work on the plasma and vice versa. Taking the conventional coordinate system where the shock normal is in the - x direction and the magnetic field lies in the x - z plane, it is straightforward to see that a component of current in the y direction exists in the shock transition layer. From Maxwell's Equations we have

$$\vec{j} = \frac{c}{4\pi}\vec{\nabla}\times\vec{B}$$

$$j_y = -\frac{c}{4\pi}\frac{\partial B_z}{\partial x} \tag{1}$$

and since, in the normal incidence frame (NIF), there is a component of the electric field in the y direction given by

$$E_y^N = \frac{1}{c}v_{1x}B_{1z} \tag{2}$$

where the subscript 1(2) refers to the upstream(downstream) side of the shock, we can see that there can be a transfer of energy from the plasma to the fields given by

$$\vec{E}\cdot\vec{j} = E_y j_y = -\frac{c}{4\pi}E_y\frac{\partial B_z}{\partial x}$$

and since E_y is continuous through the shock for a steady state

$$= -\frac{c}{4\pi}\frac{\partial}{\partial x}\left(E_y B_z\right) = -\frac{c}{4\pi}\vec{\nabla}\cdot\left(\vec{E}\times\vec{B}\right). \tag{3}$$

The energy lost by the charged particles is gained by the electromagnetic fields and is manifest as the increase of the Poynting flux. The above result is determined solely by the Rankine-Hugoniot relations i.e. by the asymptotic states of the shock transition.

Thus far no reference to B_y has been needed in deriving the energy discrepancy. This does not mean that the out-of-the-plane excursion of the magnetic field plays no role in the energetics of the situation. If the shock is viewed in the de-Hoffman Teller (HT) frame of reference the electric field in the x direction is changed by an amount δE_x where

$$\delta E_x = -\frac{1}{c} V_{HT} B_y \tag{4}$$

and the de-Hoffman Teller velocity is that transformation velocity in the z direction that makes the plasma flow along the magnetic field direction in front of and behind the shock. It is given by

$$V_{HT} = c E_y^N / B_x \tag{5}$$

Since in the HT frame there is no electric field in the y direction, and hence no Poynting flux, there can be no energy transfer between the plasma and field and any energy lost by the ions in traversing the shock potential jump must be gained by the electrons. To determine the value of this energy change we need the value of B_y.

This value can be derived by noting that when the ions and electrons pass through the shock they must receive equal increments of velocity in the z direction otherwise there would be a residual current in the z direction implying a build up of B_y in the post shock region. This can be expressed as

$$-\frac{e}{m_i c}\int (v_{iy} B_x - v_{ix} B_y) dt_i = \frac{e}{m_e c}\int (v_{ey} B_x - v_{ex} B_y) dt_e \tag{6}$$

where dt_i and dt_e are the times of travel through the shock for ions and electrons respectively. Since $v_{ix}dt_i = v_{ex}dt_e = dx$ we may write equation (6) as

$$-\frac{e}{m_i c}\int \left(\frac{v_{iy}}{v_{ix}} B_x - B_y\right) dx = \frac{e}{m_e c}\int \left(\frac{v_{ey}}{v_{ex}} B_x - B_y\right) dx \tag{7}$$

rearranging terms and making use of the fact that Bx is continuous through the shock we obtain

$$B_y dx = \frac{B_x}{(m_i + m_e)}\int \left(m_e \frac{v_{iy}}{v_{ix}} + m_i \frac{v_{ey}}{v_{ex}}\right) dx \tag{8}$$

We note that if the masses of the ions and electrons were equal, by symmetry, the current in the y direction would be carried equally by both species and their y components of velocity would be equal in magnitude and opposite in sign. Thus the right hand side of equation (8) would vanish and the integral value of B_y would be zero.

In fact the ions are much more massive than the electrons and their component of velocity in the y direction may be neglected when compared with that of the electrons especially when we see that electron velocity is weighted with the ion mass and vice versa. Since we may approximate the current in the y direction by $j_y = -en_e v_{ey}$, where n_e is the electron density, we may write equation (8) as

$$\int B_y dx = -\frac{B_x}{e n_e v_{ex}}\int j_y dx \tag{9}$$

With this approximation for B_y we find that the energy gained by the electrons in the HT frame is given by

$$
\begin{aligned}
en_0 v_{0x} E_x &= n_0 v_{0x} \int \left(E_x^N - \delta E_x\right) dx \\
&= en_0 v_{0x} \left[\int E_x^N dx - \int \left(-\frac{1}{c} V_{HT} B_y \right) dx \right] \\
&= en_0 v_{0x} \int E_x^N dx - \int E_y^N j_Y dx \qquad (10)
\end{aligned}
$$

which is precisely the amount gained in the NIF.

We see that we obtain exactly the result of Goodrich and Scudder from a different point of view.

3 Conclusion. Goodrich and Scudder argued from the requirement that electron energy gain be the same in the two frames to the existence of the y component of the magnetic field. We, on the other hand argue that B_y must exist in order to give the ions a deflection in the z direction and have shown that this argument leads to the same value of this magnetic field component. This argument leads to an understanding of the necessity of this component from the asymptotic properties of the shock and gives a simple expression for computing its value.

4 References

Ellison, D. C., F. C. Jones, and D. Eichler, Monte Carlo simulation of collisionless shocks showing preferential acceleration of high A/Z particles, J. Geophys., 50, 110, 1981

Ellison, D. C., F. C. Jones, and D. Eichler, Monte Carlo simulation of steady state shock structure including cosmic-ray mediation and particle pressure, 18th Intnl. Conf. Cosmic Rays Conf. Papers, 2, 271, 1983

Formisano, V., Measurements of the potential drop across the earth's collisionless bow shock, Geophys. Res. Lett., 9, 1033, 1982

Goodrich, C. C., and J. D. Scudder, The adiabatic energy change of plasma electrons and the frame dependence of the cross-shock potential at collisionless magnetosonic shock waves, J. Geophys. Res., 89, 6654,1984

Greenstadt, E. W., et al., A macroscopic profile of the typical quasi-perpindicular shock: ISEE 1 and 2, J. Geophys. Res., 85, 2124, 1980

Ogilvie, K. W., M. A. Coplan, and R. D. Zwickle, Helium, hydrogen, and oxygen velocities observed on ISEE 3, J. Geophys. Res. 87, 7363, 1982

SH-5.2-3

X-RAY AND RADIO EMISSION IN SOLAR ^{3}HE-RICH EVENTS

D. V. Reames
NASA/ Goddard Space Flight Center, Greenbelt, MD, USA

R. P. Lin
Space Sciences Laboratory, University of California, Berkeley, CA, USA

R. L. Stone and B. R. Dennis
NASA/ Goddard Space Flight Center, Greenbelt, MD, USA

Abstract

We have examined radio and X-ray properties of solar flares associated with a new sample of individually-identified ^{3}He-rich solar-particle events. Given the association between kilometric type III bursts and ^{3}He-rich events, the timing of the radio events is used to identify the related X-ray increases. Examination of these events shows correlations among the radio, X-ray and particle parameters. The sense of these correlations is that larger ^{3}He/^{4}He ratios occur in smaller flares suggesting that waves required for ^{3}He enhancment are damped in large, energetic flares.

1. Introduction. For many years the properties of the small and elusive ^{3}He-rich solar particle events could only be observed by integrating particle intensities for periods of many hours (see e.g. Ramaty, 1980; Kocharov and Kocharov, 1984). Therefore, these early "events" frequently combined the output of several solar flares with differing intensites and composition.

Using more sensitive instrumentation on ISEE-3, Reames, von Rosenvinge and Lin (1985, hereafter RvL) were able to resolve ^{3}He-rich periods into sequences of individual events, each accompanied by an electron increase. The precise timing of the electron increases could be used to determine the time of the parent flare with an accuracy of a few minutes. The kilometric type III radio emission produced by these same electrons was used by Reames and Stone (1986) to extend the list of well-identified ^{3}He-rich solar flares and to study the relationship of flares within a group.

In the present paper we examine, for the first time, the source properties of this new list of individual ^{3}He-rich solar flares. The same type III radio emission used to identify the events provides the timing required to select the associated hard and soft X-ray increases.

2. Observations. Particle and radio observations were made aboard the ISEE-3 spacecraft and have been described extensively in RvL and in Reames and Stone (1986). Both soft and hard X-rays were also measured aboard ISEE-3 by the Berkeley X-ray Spectrometer that covered the energy region above about 5 keV. In addition, hard X-ray measurements were made with the Hard X-ray Burst Experiment (HXRBS) on SMM. A recent summary of measurements from this instrument are given by Dennis (1986).

Of the 31 ^{3}He-rich events, 5 could not be studied completely because of data gaps or other ambiguities. For the remaining 26 events, plots like that shown in Figure 1 were prepared to study the event timing. The example in Figure 1 shows the time histories of the hard X-rays in the center panel with the radio and soft X-ray data in the upper and lower panels, respectively. Extrapolation of the radio data back (2 MHz corresponds to about 6 solar radii) to the hard X-ray peak is clear in this figure. In more complex events

the timing of the dominant radio peak was used to select the correct X-ray increase or to provide timing in cases were hard X-ray data were absent.

Of the 26 events, all showed radio increases, 20 showed soft X-ray increases and 15 showed hard X-ray increases. The X-ray profiles, like the ones in Figure 1, were extremely impulsive; soft X-ray durations (at 10% of maximum) were in the range 5-10 mins.

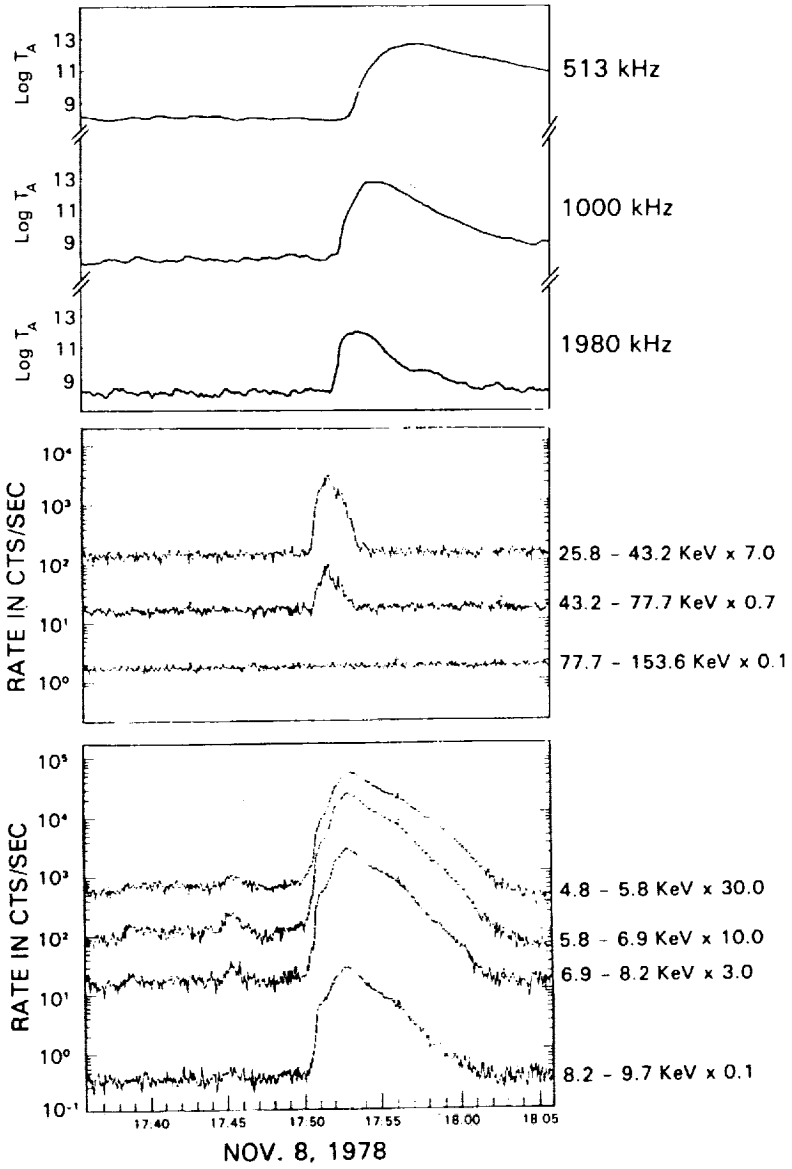

Figure 1. Radio X-ray and radio timing in the Nov 8, 1978 ^{3}He-rich event.

If one assumes that the hard X-ray time profile in Figure 1 describes the profile of particle acceleration, then the delay to the peak of the 2 MHz radio data would represent the time required for electrons to propagate out to ~6 solar radii, and the delay to the soft X-ray peak represents the time required for the accelerated particles to heat the low corona. Based on this simplistic picture, we chose the time of hard X-ray maximum to determine soft X-ray properties that might be most representative of the ambient conditions seen by the particles being accelerated.

An extremely wide range of X-ray sizes are found for the events, ranging from very large events to events with little or no detectible increase in even the softest X-rays. X-ray temperatures range from 8 to 19 x10^6 °K.

3. Results and Discussion. In Figure 2 we show cross plots of the particle, X-ray, and radio parameters for all flares in which the required measurements are available. Figure 2(a) shows $^3He/^4He$ versus the 2 MHz

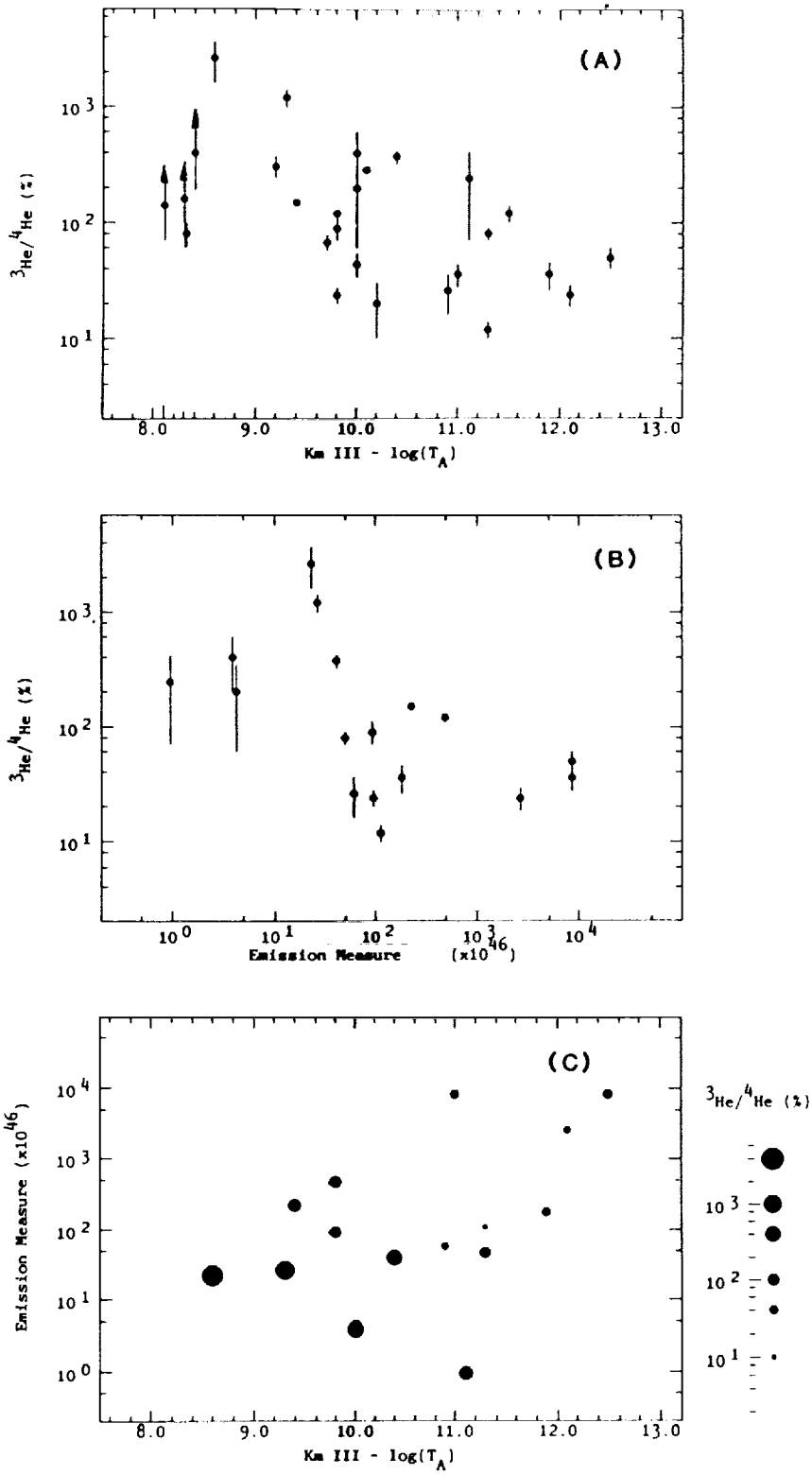

Figure 2. Cross plots of particle, radio and X-ray parameters.

intensity (log of antenna temperature) for 27 events, Figure 2(b) shows the $^3He/^4He$ ratio as a function of the soft X-ray emission measure for 17 events, and Figure 2(c) shows a cross plot of the X-ray and radio parameters with the symbol size proportional to $\log(^3He/^4He)$.

The linear correlation coefficients for the data as plotted in Figure 2 are (a) -0.520, (b) -0.533, and (c) 0.449. The corresponding probability that the variables are correlated in each case is (a) 99%, (b) 98%, and (c) 93%. However, we would not necessarily expect the underlying correlation to be either linear or simple. The figure does seem to show a tendency for higher values of $^3He/^4He$ to occur in the smaller events.

Table 1 shows correlation coefficients for several available parameters taken pairwise. The number of events contributing to each coefficient is shown in the table as is the correlation probability when it is greater than 90%. ^3He intensity was omitted from the table since it is strongly affected by the degree of magnetic connection between the event and Earth and is therefore poorly correlated.

Table 1. Correlation with $\log(^3He/^4He)$:

	Coef.	Events	Prob.
Soft X-ray Temp.	0.096	17	-
log (Soft X-ray E. M.)	-0.533	17	97%
log (Soft X-ray Peak)	-0.568	18	98%
log (SMM Hard X-ray Peak)	-0.611	11	95%
Km III log(TA)	-0.520	27	99%

The data in Table 1 show a persistent negative correlation of the $^3He/^4He$ ratio with nearly all measures of the parent event size including the hard and soft X-ray peak fluxes in addition to the parameters mentioned above. The mechanism leading to ^3He enhancment appears to operate preferentially in small events.

The existence of a correlation among event parameters seems to argue in favor of a single acceleration event rather than the decoupled pre-heating and acceleration phases suggested by Fisk (1978). Evidently the waves required for ^3He enhancement are damped in larger, more energetic events.

The authors are indebted to S. R. Kane for providing unpublished X-ray data. A portion of this work was performed under NASA grants NAG5-376 and NGL-05-003-017.

References

Dennis,B.R. 1985, *Solar Physics*, **100**, 465.
Fisk,L.A. 1986, *Ap. J.*, **224**, 1048.
Kocharov,L.G., and Kocharov,G.E. 1984, *Space Sci. Rev.*, **38**, 89.
Ramaty,R., *et al.* 1980, In: *Solar Flares, A Monograph from the Skylab Solar Workshop II*, ed. P.A. Sturrock (Colo. Assoc. U. Press), p 117.
Reames,D.V. and Stone,R.G. 1986, *Ap. J.*, **308**, 902.
Reames,D.V., von Rosenvinge,T.T. and Lin,R.P. 1985, *Ap. J.*, **292**, 716.

COSMIC-RAY VARIATIONS AND MAGNETIC FIELD FLUCTUATIONS IN THE OUTER HELIOSPHERE

J. S. Perko and L. F. Burlaga
Code 665, NASA-Goddard Space Flight Ctr., Greenbelt, Maryland, 20771, USA

Abstract

We have formally confirmed that galactic cosmic ray intensity variations measured by Voyager 2 during recovery from solar maximum are caused by travelling compressions and rarefactions in the mean interplanetary magnetic field. We used Voyager's nearly continuous magnetic field data as input to a time-independent, spherically-symmetric, cosmic-ray transport equation in the force-field approximation. The solutions closely followed the count rate of cosmic rays > 75 MeV/nucleon over four years. This strongly supports prior theoretical assertions that turbulent interaction regions travelling with the solar wind are the major cause of the solar-cycle variation of galactic cosmic rays in the ecliptic region.

1.Introduction. The search for processes that modulate cosmic rays has focussed on particle interactions with small-scale fluctuations in the magnetic field, fluctuations translated into the diffusion tensor(κ), a coefficient in the cosmic ray transport equation [10, 4]. Most attempts to solve this equation have fashioned diffusion coefficients solely to fit data, without reference to specific interplanetary conditions [12, 6]. These steady-state snapshots do show that the standard model of diffusion, convection and adiabatic deceleration is consistent with the behavior of cosmic rays in the heliosphere at fixed times. They cannot, however, describe the effect on cosmic rays of propagating interplanetary disturbances, which are the likely physical basis for the 11-year solar cycle modulation [9]. Perko and Fisk [11] modeled this effect qualitatively with a time-dependent, spherically-symmetric, numerical model, in which local decreases in κ propagate outward at solar wind speed. Their results establish propagating diffusion regions as the likeliest mechanism for solar cycle modulation near the ecliptic.

The next step was to identify these diffusion regions in the interplanetary magnetic field and plasma data. Burlaga et al. [2] found a simple correlation between the quantity B/B_P and the count rates of particles > 75 MeV/nucleon, both quantities derived from Voyager 2 data; B is the total magnetic field strength measured by the spacecraft and B_P is the mean Parker-spiral field strength. This relation is plausible, since the critical parameter κ is related to the high-frequency field fluctuations [8], and these in turn are proportional to the total field strength [1]. There is evidence then that the dominant modulation mechanism is associated with the interaction regions.

2.Model Calculation. Start with the "force-field" approximation for the cosmic ray transport equation [7, 5]

$$\frac{\partial f}{\partial r} + \frac{VP}{3\kappa}\frac{\partial f}{\partial P} \approx 0 \qquad (1)$$

where f is the number of particles per unit volume of phase space (d^3rd^3p) averaged over direction, r is the heliocentric radius, V is the solar wind speed, and P is the particle rigidity; Time is an implicit parameter. At the outer boundary r=50 AU, we assumed an interstellar proton spectrum represented by a power law in total energy with an index of -2.6.

Chih and Lee [3], in a quasilinear perturbation model, relate the diffusion coefficient to the magnetic field compression as follows: Since κ

is approximately proportional to the inverse of the wave-power spectrum at the cyclotron resonant wave number, any compression of the plasma will increase the wave power and so reduce κ. If we assume a saturated B-field fluctuation level ($\langle|\delta B|^2\rangle \propto B^2$) and a simple cutoff at the wave number $k_0 \propto B$, then $\kappa \propto B^{-1}$. This yields the desired relation

$$\delta\kappa/\kappa_0 = -\delta B/B_P \qquad (2)$$

where κ_0 and B_P are the mean, background quantities, and $\delta\kappa$ and δB are first-order deviations. In any case, functions of the form

$$\kappa \propto (B/B_P)^{-\alpha}$$

result in

$$\delta\kappa/\kappa_0 = -\alpha\ \delta B/B_P \qquad (3)$$

Equations (2) and (3) differ only in the multiplicative factor α. The use of B/B_P instead of just B removes the effect of the radial gradient of B, leaving only departures from the mean field.

To show how the magnetic field data were used in this model, note first that Voyager 2 measures the total field strength B. To get B_P, the mean Parker field, we computed a running average of B over 1/2-year intervals. The diffusion coefficient in interaction regions ($B/B_P > 1$) was set to

$$\kappa = C\ (B/B_P)^{-\alpha} \qquad (4)$$

where C and α are constants, equal to 20.0 and 0.3 respectively, and κ was assumed independent of radius. In rarefaction regions ($B/B_P < 1$), B/B_P was set to a constant 0.8. The equation for the diffusion coefficient in rarefaction regions is not known, but the rate of recovery found by Burlaga et al. [2] in each rarefaction region was constant over many such regions, despite the differences among their durations and amplitudes. Theoretically, it seems that something other than simple diffusion is driving the recovery.

Next, using the Voyager 2 magnetometer data from 1 January 1981 through 31 December 1984, we calculated hour averages of B/B_P and smoothed them with 12-hour running averages. We then compiled 8-hour averages of the smoothed data to save computer time (with little real difference in the results) and substituted these averages into equation (4), which in turn is substituted into equation (1). Next, note that a solution of equation (1) requires an integration of $V \cdot dr/\kappa$ over r from the point of observation r_V, the radius of Voyager 2, to the outer boundary of the modulation region, which we set at 50 AU; therefore κ and, in turn, B/B_P must be known as a function of distance from the sapcecraft. We did this by letting the disturbances observed at Voyager propagate outward, unchanged, at a constant speed of 500 km/s (the same as the assumed solar wind speed V), to the outer boundary of the modulation region, where their influence suddenly ends. The parameters used here in this solution are not necessarily unique, but they are consistent with current space probe data.

The procedure was to divide the radial integration region into intervals, each equal to the transit distance of the solar wind in eight hours (~0.1 AU). Then we initially set B/B_P=1 over the entire region, except at r_V, where the integration begins. There we set B/B_P to the first 8-hour average of 1 January 1981. Integrating over r from r_V to r=50 AU gave us the first solution for the cosmic-ray intensity, which we compare to the count actually measured by the spacecraft. Then the B/B_P value at r_V was advanced to the next spatial interval (~0.1 AU), the second 8-hour average for 1 January 1981 took its place at r_V, and equation (1) was again integrated. This procedure was repeated until we reached the last B/B_P point measured in 1984. When an 8-hour-averaged B/B_P point reaches the boundary at 50 AU, it disappears and is no longer contained in the integration.

3.Results & Discussion. The results of the calculation for the recovery years 1981 through 1984 are shown in Figure 1. The horizontal axis is time in years and the vertical axis is particle intensity in arbitrary units. The light line represents the model results; the dark line represents the high-

energy cosmic ray count rate from the Caltech/University of New Hampshire/Goddard Space Flight Center experiment on Voyager 2. The data are normalized to coincide with the model calculation. (The normalization is actually within about 10% of the normalization done just by requiring the leftmost points in the two curves to match.) In general, the agreement between the predicted and the observed counting rate is surprisingly good. Notice that many of the individual features in the data can be identified in the model results. Though at times the model seems out of phase with the data, this is probably caused by the use of a constant solar wind speed: Although 500 km/s is a good approximation, the actual value typically varies by 100-200 km/s.

One exception to the close fit is the gap in 1984. The predicted intensities are higher than observed, caused by strong recoveries in the model that do not occur in the data. Note that the duration of the discrepancy is approximately the solar wind transit time from the spacecraft to the outer boundary. The anomaly in the plasma and field data that misled the model probably left the system at the end of this interval. We do not see anything unusual in the plasma or magnetic field data during this time interval, except that the rarefactions may be somewhat weaker than at other times.

In this model, the treatment of cosmic ray recovery within rarefaction regions is empirical. We tried substituting into equation (4) the actual value of B/B_P in cases where $B/B_P < 1$, and the result was exaggerated recoveries in the model (not shown). So the recovery of the particles does not seem a strong function of the strength of the rarefactions.

The actual cause of the cosmic ray scattering is probably magnetic field fluctuations, e.g., turbulence and discontinuities [2]. Two rough measures of these fluctuations are σ_B, the root mean square (r.m.s.) variance in the total magnetic field strength in an hour interval, and σ_c, the r.m.s. variance in the field components in an hour interval. Figure 3 shows Voyager 2 observations of the averages of σ_B and σ_c as a function of B, where B is the average magnetic field strength for the interval 1981.0 to 1985.0. Both σ_B and σ_c increase with B, showing that regions with strong magnetic fields tend to have a higher level of fluctuations than regions with weak fields. Although it is desirable to relate κ to σ_B and σ_c, we know of no derivation of such a relation. Solutions of equation (1) with $\kappa \propto (\sigma_B/B_P)^{-\alpha}$ or $\propto (\sigma_c/B_P)^{-\alpha}$ failed to reproduce observed intensity profiles.

4.Conclusion. The assumptions of Chih and Lee's [3] quasilinear perturbation model--a saturated magnetic fluctuation level and a simple wave-number cutoff ($k_0 \propto B$) in the magnetic field power spectrum--appear reasonable. Using these assumptions, our results show that solutions of the force-field approximation to the cosmic ray transport equation with a diffusion coefficient related to the observed magnetic field strength agreed well with short- and long-term trends in cosmic ray intensity, at least during periods when the heliosphere is recovering from solar maximum. Therefore, even though particle scattering may be most closely related to the small-scale field fluctuations, B/B_P accurately represents the size and power of long-lived, large-scale, turbulent scattering regions, which are responsible for cosmic ray intensity trends in the ecliptic down to a time scale of weeks, and which span at least the recovery phase of a solar cycle. Unfortunately, the model does not seem to work in the declining phase of the cosmic-ray cycle. As a model for the whole 11-year cycle, it is oversimplified, especially between 1 and 10 AU, the location of Voyager 2 from 1977-1981, where there are fast flows that interact strongly with one another. This model most likely simulates only the merged flows that exist beyond 10 AU.

5.Acknowledgements. We thank N. F. Ness for providing the field data used in this study, and F. B. McDonald for providing the cosmic ray data.

References

1. Burlaga et al., J. Geophys. Res., 87, 4345, 1982.
2. Burlaga et al., J. Geophys. Res., 90, 12,027-12,039, 1985.
3. Chih, P.-P., and M. A. Lee, J. Geophys. Res., 91, 2903-2913, 1986.
4. Fisk, L. A., in Solar System Plasma Physics, Vol. 1, ed. Parker et al., pp. 177-247, North-Holland, New York, 1979.
5. Fisk et al, J. Geophys. Res., 78, 995-1006, 1973.
6. Garcia-Munoz et al., Proc. Int. Conf. Cosmic Rays 19th, 4, 409-412, 1985.
7. Gleeson, L. J., and W. I. Axford, Astrophys. J., 154, 1011-1026, 1968.
8. Jokipii, J. R., Rev. Geophys. Space Phys., 9, 27-87, 1971.
9. McDonald et al., Astrophys. J., 249, L71-75, 1981.
10. Parker, E. N., Planet. Space Sci., 13, 9-49, 1965.
11. Perko, J. S., and L. A. Fisk, J. Geophys. Res., 88, 9033-9036, 1983.
12. Urch, I. H., and L. J. Gleeson, Astrophys. Space Sci., 17, 426-446, 1972.

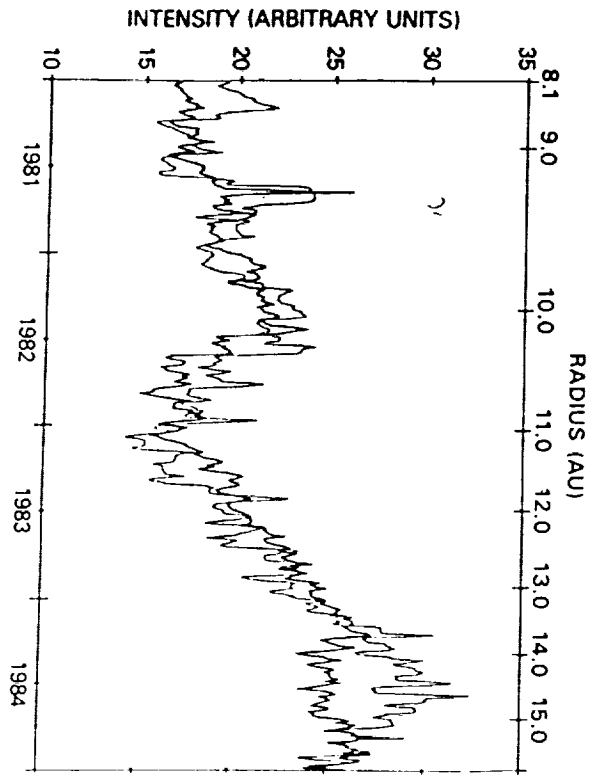

Figure 1.Voyager particle count (>75 MeV, heavy line); force-field results(light line); vertical axis is arbitrary intensity; horizontal axis is years; data normalized to model results.

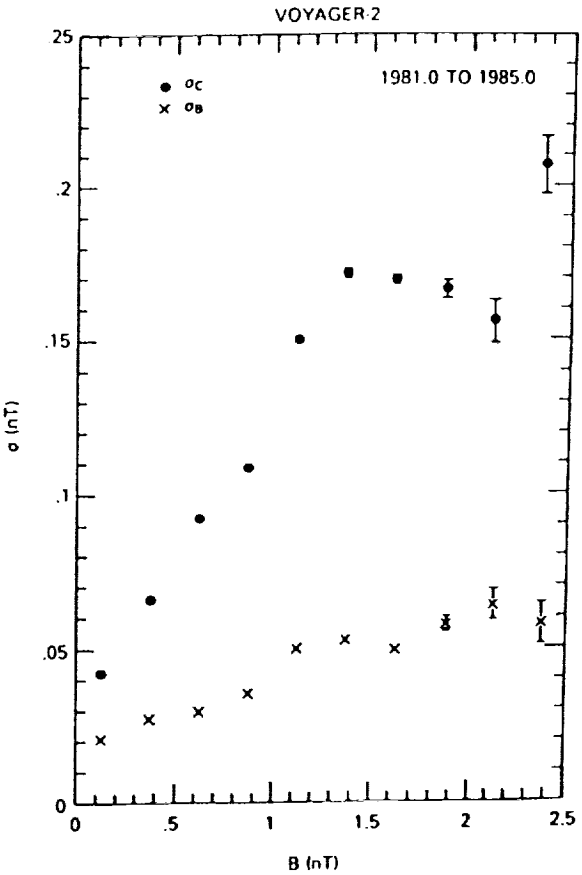

Figure 2.Average r.m.s. fluctuations in strength(σ_B) and direction(σ_C) of magnetic field in hour intervals, measured by Voyager 2 from 1981.0 to 1985.0, as a function of hourly average of strength of magnetic field; bars are errors in mean of σ.

SH 6.4-10

THE REAPPEARANCE OF THE ANOMALOUS OXYGEN COMPONENT AT 1 A.U.

T. T. von Rosenvinge and D. V. Reames
NASA/Goddard Space Flight Center, Greenbelt, MD, USA

Abstract

The anomalous oxygen component has been observed to reappear at the ICE spacecraft at 1 A.U. in the period March 1- May 1, 1986. The prediction of a strong decrease in intensity of the anomalous component in alternate solar cycles (4) is not borne out. The observations suggest that the anomalous component is singly charged in accordance with the predictions of Fisk *et al.* (3).

1. Introduction. The anomalous component of the low energy cosmic rays is characterized by an oxygen to carbon ratio which can exceed 10 at about 10 MeV/n (1). Anomalous oxygen was first discovered in 1971 and disappeared in early 1978 with the onset of solar maximum. Fisk *et al.* (2) suggested that the anomalous elements are interstellar neutrals which come into the inner heliosphere, are ionized, and then become accelerated in the outer heliosphere. This theory correctly predicted the enhancement of Neon at low energies (3). The further prediction that the anomalous oxygen is singly charged has not been well verified, however. Extensions to the original theory of Fisk *et al.* have been discussed by Pesses *et al.* (4) and by Jokipii (5). Pesses *et al.* predicted a strong decrease in the intensity of the anomalous component in alternating 11-year solar cycles. In this paper we present evidence that the anomalous oxygen component is in fact recovering as solar minimum conditions are reappearing.

2. Observations. We report on observations made from the ISEE-3/ICE spacecraft at 1 A.U. during the period March 1-May 1, 1986 (excluding some solar active days). Energy spectra for protons, He and oxygen are shown in Figure 1. The proton spectrum turns up at the lowest energy point indicating solar particles; the He spectrum at the same kinetic energy/n shows no turn up, however, and contamination of the oxygen spectrum is negligible. Figure 1 shows the oxygen intensity in the lowest energy interval as measured in two independent telescopes. Note the flat He spectrum below 100 MeV/n, reminiscent of the He spectrum during the last solar minimum.

In Figure 2 we compare the oxygen spectrum from Figure 1 with that measured at 1 A.U. in the period November, 1973-May, 1974 (3). The recent spectrum is apparently somewhat steeper than the earlier one and roughly a factor of 3 lower. Figure 4 shows the Deep River neutron monitor intensity from 1970 to the end of 1986. The neutron monitor levels were about the same for the two spectra shown in Figure 2.

3. Discussion. Two earlier searches (6,7) for the reappearance of the anomalous oxygen reported only upper limits. For example, Mason *et al.* (7) reported an upper limit in 1984 of $\sim 10^{-6}$/cm^2-sr-sec-MeV/n for oxygen in the energy interval 6.6-12 MeV/n. This may be compared with our measured value of $0.8 \pm .2 \times 10^{-6}$/cm^2-sr-sec-MeV/n in essentially the same energy interval. As noted in (7) and as may be seen in Figure 4, the neutron monitor levels in

1984 had not yet returned to the level at which the anomalous component "disappeared" in 1978 so it is not surprising that the earlier searches failed to detect the reappearance of the anomalous oxygen.

In early 1986 the neutron monitor levels had just returned to the levels of the previous solar minimum (~1971-1977). Figure 3 shows the intensity of 187-447 MeV/n He as a function of time together with the level which prevailed in 1977. Figure 3 suggests that the He intensity in this energy interval will not recover to the levels of the previous solar minimum until early 1987, i.e. one year later than when the neutron monitor recovered. If a similar hysteresis applies to the anomalous oxygen component, then we may expect that the oxygen intensity will also continue to recover and will probably reach the same intensity level as during the last solar minimum. If this is correct, then the predictions of Pesses *et al.* (4) are not borne out.

Calculations are in progress which model the propagation of the He and oxygen intensities observed at Pioneer 10 in early 1986 (~37 AU) to 1 AU using a spherically symmetric diffusion-convection modulation model. The resulting spectra are a close match to the He and oxygen spectra shown in Figure 1, provided that the low energy He and oxygen are both considered to be singly charged.

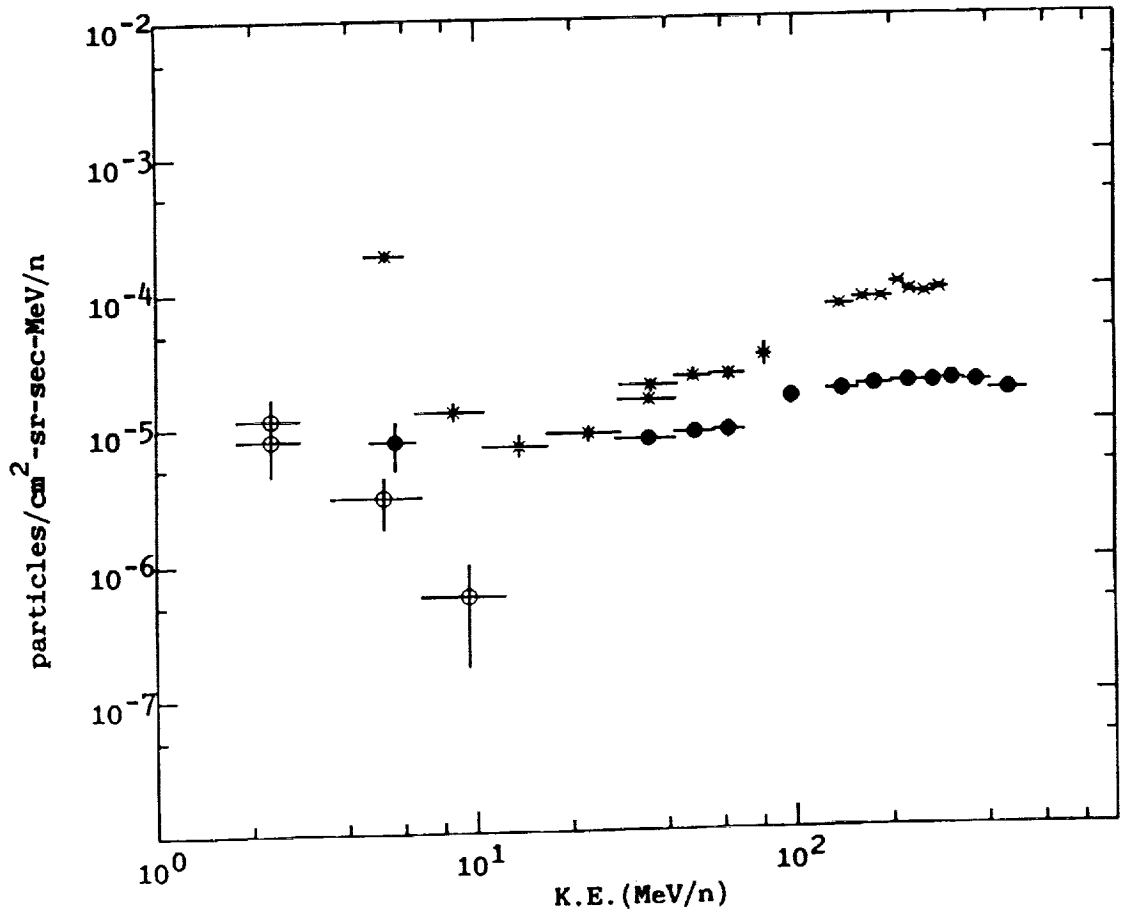

Figure 1. Energy spectra from ISEE-3/ICE during March 1-May 1, 1986 (crosses-protons; solid circles-He; open circles-oxygen).

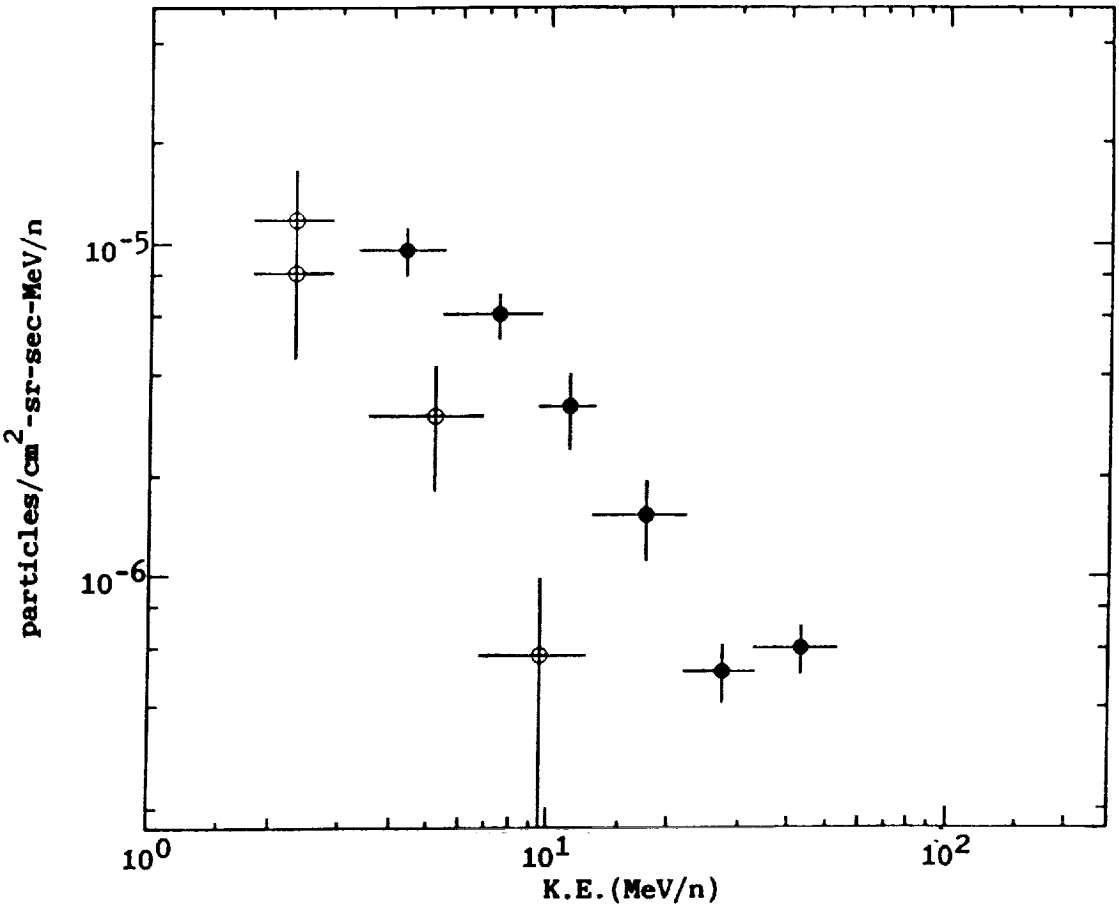

Figure 2. Oxygen energy spectra at 1 AU (open circles-from Figure 1; solid circles-November, 1973-May, 1974).

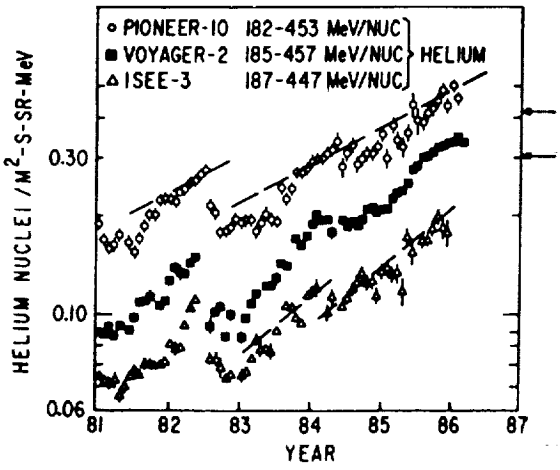

Figure 3. Time histories (26 day averages) of the helium intensities at Pioneer 10, Voyager 2 and ISEE-3. The arrows on the right hand side indicate the intensities recorded at the 1977 solar minimum period at 1 and 15 AU. From reference (8).

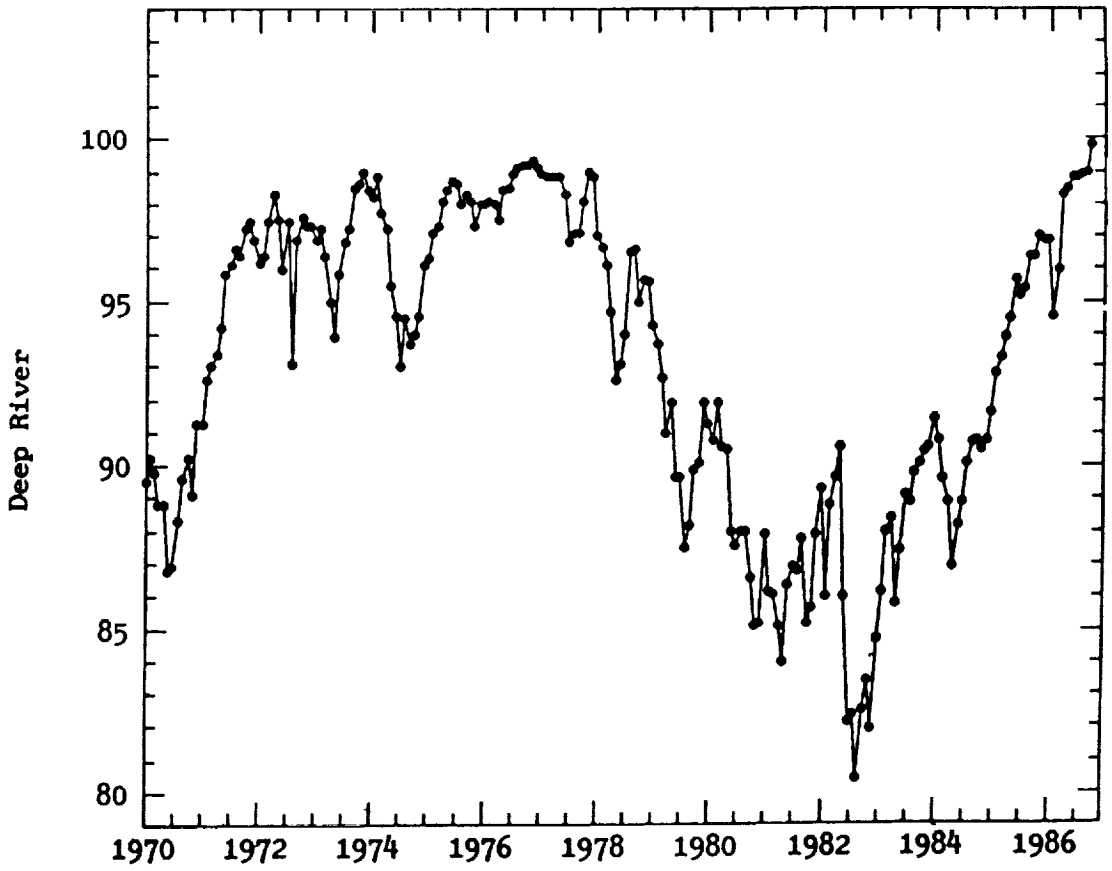

Figure 4. Monthly average values of the Deep River neutron monitor counting rate normalized to 100% in May, 1965 (solar minimum).

References

1. McDonald, F.B., Teegarden, B.J., Trainor, J.H. and Webber, W.R., *Ap. J.(Letters)*, 187, L105, 1974.
2. Fisk, L.A., Kozlovsky, B., and Ramaty, R., *Ap. J.(Letters)*, 190, L35, 1974.
3. von Rosenvinge, T.T. and McDonald, F.B., 14th ICRC, 2, 792, 1975.
4. Pesses, M.E., Jokipii, J.R., and Eichler, D., *Ap. J.(Letters)*, 246, L85, 1981.
5. Jokipii, J.R., *JGR*, 91, 2929, 1986.
6. Mewaldt, R.A., and Stone, E.C., 19th ICRC, 5, 167, 1985.
7. Mason, G.M., Klecker, B., Galvin, A.B., Hovestadt, H., and Ipavich, F.M., 19th ICRC, 5, 168, 1985.
8. McDonald, F.B., von Rosenvinge, T.T., Lal, N., Trainor, J.H., and Schuster, P., *Geophys. Res. Lett.*, 13, 785, 1986.